© 2024. Published by The Company of Biologists Ltd.
This is an Open Access article distributed under the terms of the Creative Commons Attribution License http://creativecommons.org/licenses/by /4.0), which permits unrestricted use, distribution and reproduction in any medium provided that the original work is properly attributed

Filopodial protrusion driven by density-dependent Ena-TOCA-1 interactions

Thomas C. A. Blake[1,2], Helen M. Fox[1,2], Vasja Urbančič[1,2], Roshan Ravishankar[4], Adam Wolowczyk[1,2], Edward S. Allgeyer[1,3], Julia Mason[1,2], Gaudenz Danuser[4], Jennifer L. Gallop[1,2,*]

[1]Wellcome/Cancer Research UK Gurdon Institute, University of Cambridge, Cambridge, UK
[2]Department of Biochemistry, University of Cambridge, Cambridge, UK
[3]Department of Genetics, University of Cambridge, Cambridge, UK
[4]Lyda Hill Department of Bioinformatics, UT Southwestern Medical Center, Dallas, TX 75390, USA

[*]Correspondence to Jennifer L. Gallop: j.gallop@gurdon.cam.ac.uk

Abstract

Filopodia are narrow actin-rich protrusions with important roles in neuronal development where membrane-binding adaptor proteins have emerged as upstream regulators that link membrane interactions to actin regulators, for example I-BAR and F-BAR domain-containing proteins interacting with Ena/VASP and formins. To explore the significance of the F-BAR neuronal membrane adaptor TOCA-1 in filopodia we used quantitative analysis of TOCA-1 and filopodial dynamics in *Xenopus* retinal ganglion cells, where Ena/VASP proteins have a native role in filopodial extension. Both the adaptors and their binding partners are part of diverse and redundant protein networks that can functionally compensate for each other. Increasing density of TOCA-1 enhances Ena/VASP binding *in vitro* and an accumulation of TOCA-1, and its coincidence with Ena, correlates with filopodial protrusion *in vivo*. Two-colour single molecule localisation microscopy of TOCA-1 and Ena supports their nanoscale association. TOCA-1 clusters promote filopodial protrusion depending on a functional SH3 domain and activation of Cdc42, which we perturbed using small molecule inhibitor CASIN. We propose that TOCA-1 clusters act independently of membrane curvature to recruit and promote Ena activity for filopodial protrusion.

Keywords: growth cone, actin, migration

Journal of Cell Science • Accepted manuscript

Introduction

Axonal growth cone navigation underlies accurate neuronal connectivity in the brain, guided by chemical and mechanical cues that are transduced to the cytoskeletal machinery to enable movement and turning (O'Connor et al. 1990; Koser et al. 2016). Filopodia are one key element, which protrude through the dynamic growth and shrinkage of long, unbranched bundles of actin filaments, controlled by actin regulators at the filopodia tip (Mallavarapu & Mitchison 1999; Applewhite et al. 2007; Blake & Gallop 2023). In the axonal growth cone, stochastic protrusion of filopodia has roles in transient adhesion to surfaces and promoting accurate movement (O'Connor et al. 1990; Dwivedy et al. 2007). Control of filopodial protrusion, retraction and adhesion allows cells to transduce signals and transmit force to the environment via an adhesion-based molecular clutch (Chan & Odde 2008; He et al. 2017). The actin bundle is surrounded by high negative curvature plasma membrane that is stabilised by proteins that link curved plasma membrane to the cytoskeleton such as IRSp53 (Nakagawa et al. 2003; Mattila et al. 2007; Tsai et al. 2018). How the process of filopodial protrusion is controlled is important for understanding the mechanistic and genetic basis of intellectual disabilities and autism amongst other conditions (Truesdell et al. 2015; Hu et al. 2016; Gouder et al. 2019; Wit & Hiesinger 2022). As an established axon guidance model, here we used *ex vivo* dissected primary *Xenopus* retinal ganglion cells to elucidate the mechanisms of filopodial extension. In embryos, these growth cones migrate from eye primordia along a laminin matrix to the tectum in the brain and when explanted onto laminin-coated dishes they migrate with large growth cones and are amenable to high temporal and spatial resolution imaging (Koser et al. 2016; Urbančič et al. 2017).

Many actin regulatory proteins that contribute to filopodial growth, including Ena/VASP proteins and myosin-X, have been shown to localise to filopodia tips and their depletion or knockout alters the number or length of filopodia, revealing they play a direct or indirect functional role (Lebrand et al. 2004; Barzik et al. 2014; Jacquemet et al. 2019; Pokrant et al. 2023). Initiation pathways of filopodia have been proposed based on recruitment of membrane adaptor protein IRSp53, which deforms the membrane and in turn recruits VASP to elongate actin filaments (Disanza et al. 2013; Sudhaharan et al. 2019; Tsai et al. 2022). Dynamic complexes of another initiating membrane adaptor, lamellipodin, with VASP have also been shown to grow to a defined stoichiometry for controlled and productive

Journal of Cell Science • Accepted manuscript

protrusion (Cheng & Mullins 2020). Ena/VASP family proteins determine force generation and actin architecture in lamellipodia (Bear et al. 2002; Damiano-Guercio et al. 2020) and are localised to the growing tip of filopodia where their presence correlates with new actin monomers being incorporated into the elongating bundle (Applewhite et al. 2007; Urbančič et al. 2017). Biochemically, Ena and VASP are processive actin elongating proteins requiring G-actin binding activity, F-actin binding activity and oligomerisation for their function (Breitsprecher et al. 2008; Hansen & Mullins 2015; Harker et al. 2019) and are regulated by post-translational modifications including ubiquitination (McCormick et al. 2023).

It remains unclear how interaction partners and mechanisms combine to control Ena or VASP activation, since neither IRSp53 nor lamellipodin are essential for Ena or VASP recruitment (Pokrant et al. 2023). What triggers filopodial formation at certain sites and when filopodia grow or retract is unknown. Other candidate membrane adaptors that localise to filopodia are the neuronally-enriched TOCA-1/FNBP1L family that includes FBP17 and paralogue CIP4 (present in mammals though not in *Xenopus*), which promote lamellipodial, filopodial and neurite formation in conjunction with GTP-bound Cdc42, N-WASP and WAVE (Ho et al. 2004; Kakimoto et al. 2006; Bu et al. 2009; Fricke et al. 2009; Hu et al. 2011; Saengsawang et al. 2012, 2013). TOCA-1 has previously been studied in EGFR-activated A431 epidermoid carcinoma cells where it has EGFR-dependent roles in filopodia, endocytosis and cell motility (Hu et al. 2011). In mouse cortical neurons, TOCA-1 family members each promote or oppose neurite formation and endocytosis depending on the isoform expressed (Taylor et al. 2019). In these neurons, but not in COS7 cells, CIP4 localises to the tips of extending filopodia and is proposed to interact with Ena (Mena) as well as formin DAAM1, phosphoinositide lipids and uncapped actin to promote the formation of bundled actin structures in axonal growth cones (Saengsawang et al. 2012, 2013).

There is conflicting evidence about whether TOCA-1 contributes positively or negatively to filopodial protrusion since TOCA-1 overexpression induced filopodial formation (Bu et al. 2009) while TOCA-1 knock-down or CIP4 knock-out increased filopodia numbers (Hu et al. 2011; Saengsawang et al. 2012). Because of their positively curved F-BAR domains TOCA-1 family proteins have been implicated more in endocytic scenarios (Tsujita et al. 2006; Bu et

Journal of Cell Science • Accepted manuscript

al. 2009; Giuliani et al. 2009; Feng et al. 2010; Ledoux et al. 2023) and any role at filopodia tips would seem inconsistent with the proposed curvature sensitivity.

Distinguishing between different mechanistic functions suggested by genetic or chemical perturbation can be complex. In filopodia, upregulation of formins FMNL2 and FMNL3 takes place after acute removal of Arp2/3 complex member Arp3, inducing filopodial formation (Dimchev et al. 2021). Conversely, IRSp53 and other I-BAR proteins can generate filopodia but are not essential (Pokrant et al. 2023). Altering the level of G-actin sequestering protein profilin 1 to different extents leads to mass changes in cellular filopodial or lamellipodial architecture, distinct from a model where proteins are limited to specific roles in generating individual filopodia (Skruber et al. 2020). As well as competition between the distinct, interconnected F-actin networks in the cell for actin monomers (Burke et al. 2014; Dimchev et al. 2017; Kadzik et al. 2020), redundancy and stochasticity in regulatory protein composition and dynamics have themselves been implicated as key underlying mechanisms in filopodial generation (Dobramysl et al. 2021; Mancinelli et al. 2021).

Quantitative image analysis employing cross-correlation analysis and fluctuation analysis of protein recruitment alongside morphological changes offers the opportunity to: (1) investigate a protein within its physiologically relevant spatio-temporal context and interaction network (2) analyse 'non-essential' proteins (such as TOCA-1) where knockdown/knockout approaches do not reveal a decisive phenotype and (3) where a protein has multiple proposed functions from perturbation experiments, to study each proposed function individually and distinguish scenarios where the protein has a functional role distinct from localisation alone (Welf & Danuser 2014; Lee et al. 2015). Recent work analysing the regulation of actin dynamics in lamellipodia demonstrates how Granger Causality Analysis extracts *bona fide* cause-effect relations from imaged time series, distinguishing between proteins that drive lamellipodial extension and proteins that are present but do not functionally contribute such as a polymerisation-deficient VASP mutant (Noh et al. 2022).

Filopodia represent a powerful system for employing these methods because filopodial protrusion is a fast-moving morphological readout for dynamic changes in protein

Journal of Cell Science • Accepted manuscript

recruitment and their shape means they are an easily definable object to analyse. In previous work we used cross-correlation analysis to demonstrate that Ena and VASP arrival at filopodia precedes future protrusion in a significant subset of filopodia, recapitulating insights from knockout studies for Ena and VASP in the absence of genetic perturbation (Urbančič et al. 2017). Here, to address the role of F-BAR protein TOCA-1 in filopodial formation we have used a combination of *in vitro* binding assays, cross-correlation and Granger Causality Analysis of filopodial dynamics, and perturbation of Cdc42 using small molecule inhibitor treatment to demonstrate the contribution of TOCA-1 to Ena recruitment and filopodial extension. We show that the coincidence of TOCA-1 and Ena at lamellipodia and filopodia tips precedes forward filopodial movement in native filopodia and propose a density-dependent switch in TOCA-1 binding to Ena at the start of cycles of filopodial protrusion.

Results

TOCA-1 interacts with Ena and VASP in a density-dependent manner and localises to filopodia

Within a cell-free model of filopodia-like structures that uses *Xenopus* egg extracts applied to supported lipid bilayers to produce fascin-bundled actin structures (Lee et al. 2010), the abundance of TOCA-1 has a notable correlation with the abundance of Ena and VASP at sites of actin incorporation (Dobramysl et al. 2021). To determine whether TOCA-1 is capable of interaction with Ena and VASP directly, we covalently coupled recombinant SNAP-tagged *Xenopus tropicalis* TOCA-1, or SNAP alone, to benzylguanine-derivatised magnetic beads and incubated them with *Xenopus* egg high speed supernatant extracts. SNAP-TOCA-1 beads precipitated known interaction partners N-WASP and Diaph3, plus Ena and VASP (Fig. 1A).

The TOCA-1 family of proteins forms both dimers and higher order oligomers on membranes where it clusters monomeric N-WASP via its SH3 domain interaction (Frost et al. 2008; Padrick & Rosen 2010). Ena and VASP contain a tetramerization domain and their increased clustering scales with their processivity of actin filament elongation (Breitsprecher et al. 2008; Harker et al. 2019). Therefore, we tested whether the interaction of TOCA-1 with N-WASP, Ena or VASP differs in response to the level of clustering of TOCA-1 (Fig. 1B).

Journal of Cell Science • Accepted manuscript

We mimicked the effect of TOCA-1 clustering on membranes by tuning the density of SNAP-TOCA-1 on beads and incubating them with extract to mimic cytosol, under these conditions the concentrations are N-WASP 71 nM, VASP 70 nM and Ena 132 nM (Dobramysl et al. 2021). 1 nmol of SNAP-TOCA-1 was used at different densities on the beads in a 0.4 ml assay volume, resulting in a 10-30-fold excess of TOCA-1 binding sites to any single binding partner (each present at ~30-90 pmol). While all the N-WASP was bound by a fixed quantity of TOCA-1 regardless of whether it was sparsely or densely coupled to beads, Ena and VASP showed a strong preference for a dense coupling of TOCA-1 (Fig. 1C), suggesting that in cells with the array of binding partners, Ena and VASP might interact dynamically with TOCA-1 only when it reaches high density.

TOCA-1 has previously been seen to localise to and stimulate filopodia in N1E-115 neuroblastoma cells and mouse cortical neurons (Bu et al. 2009; Saengsawang et al. 2012). To verify that endogenous TOCA-1 localises to natively forming filopodia in our system we performed immunostaining of *Xenopus* retinal ganglion cell (RGC) axonal growth cones finding that endogenous TOCA-1 localises to the tips and shafts of filopodia (Fig. 1D, Fig. S1). In RGCs expressing mNG-Ena, immunostaining of endogenous TOCA-1 revealed that, while TOCA-1 and Ena puncta are often distinct, many filopodia shafts and tips contain both TOCA-1 and Ena (Fig. 1D). We quantified the areas of overlap finding typically 1-3 per filopodium and a higher frequency of overlap puncta in shorter filopodia (Fig. 1E). To quantify the dynamics of TOCA-1 recruitment to filopodia, we expressed mNG-TOCA-1 and membrane marker GAP43-RFP in RGCs, revealing the dynamics of TOCA-1 at filopodia tips, advancing lamellipodia and to inwardly-moving puncta within the central domain (Fig. 1F; Movie 1). Across all filopodia at any given timepoint, 64% of filopodia had TOCA-1 present in the shaft or tip (mean of 3 frames, from 11 growth cones with 53 filopodia on average). Of newly-forming filopodia, 65% had TOCA-1 at the tip. In 41% of filopodia, TOCA-1 could be seen departing from the base of the filopodium during formation (17 filopodia from 5 growth cones), similar to the splitting of filopodial initiation complexes implicated in maintaining lamellipodin-VASP stoichiometry (Cheng & Mullins 2020). Tracking individual TOCA-1 plasma membrane-localised puncta over four-minute time-lapse videos revealed that 46% persisted at the plasma membrane not at a filopodium, 34% moved inwardly to

Journal of Cell Science • Accepted manuscript

the central domain and 21% localised to filopodia, either at the tips or mobile within the shaft (107 TOCA-1 puncta from 4 growth cones).

Given the positive curvature sensing of the F-BAR domain seemingly opposite to the curvature of filopodia tips, we wanted to determine whether the localisation of TOCA-1 to filopodia tips was functionally significant. Inspection of the lamellipodial TOCA-1 puncta that went on to form filopodia revealed they increased in fluorescence density in the few seconds before filopodium formation. In 14/26 filopodia, 2-3 distinct puncta of TOCA-1 coalesced in the few seconds before formation, forming a single bright punctum which usually stayed at the tip (Fig. 1G, Movie 2). Across all formation events, TOCA-1 fluorescence intensity at the site of formation increases in the -20 to -10 s prior to protrusion and then drops before tip emergence (-5 to -2 s) (Fig. 1H). This is earlier than Ena which peaks at -2 s and only drops as the tip emerges (Urbančič et al. 2017), suggesting that dense TOCA-1 transiently accumulates at the initiation of filopodia, where it could interact with Ena.

Quantification of TOCA-1 fluorescence with filopodial protrusion demonstrates a similar relationship to filopodial movement as Ena

Having established that TOCA-1 and Ena/VASP undergo a density-dependent interaction *in vitro* and partially overlap in cells, we analysed filopodia from 11 growth cones expressing mNG-TOCA-1 using our semi-automated analysis pipeline, Filopodyan, to compare the behaviour of TOCA-1 to Ena or VASP in filopodial extension and other dynamic behaviours. In our previous analysis of Ena and VASP in ongoing filopodial protrusion we used cross-correlation analysis to identify sub-populations of Ena and VASP-responding filopodia showing that their fluorescence at filopodia tips correlates with tip extension (Urbančič et al. 2017).

By measuring tip movement speed alongside tip mNG-TOCA-1 fluorescence at each time point (Fig. 2A,B), we calculated a cross-correlation function (CCF) score for each filopodium, scoring from +1 (perfect positive correlation) to -1 (perfect negative correlation). To identify any offset in peak tip fluorescence relative to tip movement, CCFs were calculated across a range of time offsets, from -40 to +40 s, followed by hierarchical clustering of the filopodia by their CCF scores (Fig. 2C). A continuum is seen between weak negative correlation, weak

Journal of Cell Science • Accepted manuscript

positive correlation, and, for a sub-cluster of 35/88 “TOCA-1 responding” filopodia, strong positive correlation, similar to our previous findings with Ena and VASP. For most of the TOCA-1 responding filopodia, the CCF scores were significantly higher than expected by chance, tested with a Markov chain-based simulation (simulated CCFs exceeded observed in <500/10,000 cases for 23/35 in sub-cluster 1; Fig. 2C). RGCs expressing the levels of mNG-TOCA-1 we are imaging had no significant differences in any of the measured dynamic parameters compared to expression of mNG alone (Fig. S2, Table S1).

On average, the TOCA-1 responding filopodia had peak correlation between TOCA-1 tip fluorescence and tip movement at an offset of -2 s prior to forward tip movement (mean CCF = 0.36, Fig. 2D). This difference in cross-correlation score between the sub-clusters was robust to different dividing points (Fig. S3A). Exploring the dynamic properties of the two sub-clusters reveals that TOCA-1 responding filopodia have a two-fold increase in the persistence of tip movement (Fig. 2E, Table S2), and this increase was robust to varying the sub-clustering point or varying data processing parameters such as smoothing (Fig. S3B,C). Like Ena, and in contrast to VASP (Urbančič et al. 2017), the TOCA-1 responding sub-cluster had no significant change in tip extension rate (Fig. 2E), suggesting a specific function for TOCA-1 in facilitating persistent filopodial growth.

Granger causality analysis validates the TOCA-1 responding sub-population identified by cross-correlation

Correlation between protein recruitment to dynamic regions of the cell and cell morphology does not always imply functional relevance at that site. Therefore, to distinguish between situations where TOCA-1 is ‘passively’ localising to extending filopodia tips and TOCA-1 having an active functional role, we used Granger Causality Analysis (GCA), which tests whether fluctuations in a given signal (here, TOCA-1 tip fluorescence) are essential for predicting future fluctuations in another signal (tip movement). This approach infers the level of causality and hierarchy of cause and effect between two variables (Noh et al. 2022).

In essence, GCA tests whether the past values of variable A are informative to explain the future values of a variable B. To do so, the procedure relies on two regression models. The

Journal of Cell Science • Accepted manuscript

first model (the *reduced* model) describes the value of variable B at time t, B_t, as a function of the previous p values of B. The second model (the *full* model) also considers the past r values of A. The optimal lag orders p and r are determined by model selection using the Bayesian Information Criterion (BIC). The variable A is deemed causal for B if the variance of the residual variable of the second model is significantly reduced compared the variance of the residual variable of the first model. Applying this approach to the same time series of TOCA-1 tip fluorescence as variable A and filopodia tip movement as variable B we found a subset of filopodia (14/88) in which TOCA-1 fluorescence is Granger-causal for tip movement at a false discovery rate (FDR) of 0.1 (Fig. 2F).

This subset overlapped with the subset of TOCA-1-responding filopodia defined by cross-correlation scores (Fig. 2C; black arrows) confirming that both methods identify similar filopodia with functionally relevant TOCA-1. To assess the level of agreement between cross-correlation and Granger causality we grouped filopodia into sub-clusters according to the Granger causality definition, which also produced a TOCA-1 responding subpopulation with greater mean cross-correlation between tip fluorescence and tip movement (Fig. 2G). To test whether the level of cross-correlation is significant (for either approach), we prepared 1000 simulated datasets by reshuffling the order of tip movement data for each filopodium. The mean CCF for the TOCA-1 responding sub-cluster was significantly higher in the observed data than in the randomised data: 0/1000 simulations produced a TOCA-1 responding sub-cluster with higher mean CCF than the sub-cluster defined by cross-correlation and 3/1000 simulations produced a sub-cluster with higher CCF than that defined by GCA (Fig. 2H). Thus two independent statistical approaches validate the functional importance of the relationship between TOCA-1 and filopodial protrusion.

The effect of mutations in TOCA-1 supports a functional role of TOCA-1 in filopodial protrusion

To test the identified role of TOCA-1 in filopodial protrusion and tip persistence, we investigated the importance of different domains of TOCA-1. We confirmed that the SH3 domain was the major site of interaction between TOCA-1 and Ena or VASP by expressing each of the following TOCA-1 constructs, coupling them to magnetic beads and testing their

Journal of Cell Science • Accepted manuscript

ability to precipitate Ena and VASP: the F-BAR domain only, the F-BAR and HR1 domains, the F-BAR and HR1 domains with the subsequent linker region, a point mutation in the SH3 domain which abolishes the interaction between TOCA-1 and N-WASP (W517K) (Ho et al. 2004), or the SH3 domain alone (Fig. 3A). A functional SH3 domain is necessary and sufficient for Ena and VASP interactions (Fig. 3B). To confirm the interactions with TOCA-1 are direct and via the proline-rich regions (PRR) of Ena and VASP, purified recombinant *Xenopus* wildtype and ΔPRR proteins (Fig. 3A) were incubated with immobilised, purified SNAP-TOCA-1. Purified wildtype Ena and VASP bound directly to SNAP-TOCA-1 (Fig. 3C,D) and deleting the PRR of Ena reduced binding (Fig. 3C), however neither PRR deletion nor mutation of an additional proline within VASP meaningfully reduced binding (Fig. 3D). VASP does not precipitate with SNAP beads alone (Fig. 3D) suggesting either that there are other possible candidate prolines within VASP or that there is a different type of molecular interaction sequence within VASP responsible for its interaction with TOCA-1. We note however that VASP behaves differently to Ena, with VASP being more dependent on polymerised actin for recruitment to *in vitro* filopodia-like structures and showing a lower level of correlation with TOCA-1 (Dobramysl et al. 2021) as well as the dynamic differences in growth cones (Urbančič et al. 2017).

In RGCs expressing mNG-TOCA-1-FBAR or mNG-TOCA-1-W517K, TOCA-1 puncta were more diffuse and transient (Fig. 3E, Movie 3) and their filopodial localisation was slightly reduced. Across all filopodia at any given timepoint, 48% of filopodia had TOCA-1-FBAR present in the shaft or tip, and 52% had TOCA-1-W517K (mean of 3 frames, from 11 growth cones with 48 and 46 filopodia on average, respectively), compared to 64% for wild type. Expression of TOCA-1 mutants did not affect the average number of new filopodia per cell per minute (2.0 for wild type, 2.3 for TOCA-1-FBAR and 2.3 for TOCA-1-W517K) or filopodial lengths (Fig. 3F). On expression of the mutants, filopodial tip persistence was reduced significantly, from median 16 s for wild type to 6.2 s (FBAR) and 9.2 s (W517K), suggesting dominant negative effects (Fig. 3G), while filopodia bases moved faster but spent more time stalled (Fig. S3D).

To test whether the shifts in localisation pattern and filopodial dynamics were functionally important, we repeated the cross-correlation and GCA on the mutants. In both mutants, correlation between tip fluorescence and tip movement was almost completely lost (Fig.

Journal of Cell Science • Accepted manuscript

3H), and fewer filopodia showed significant Granger causality between either mutant and tip protrusion (black arrows in Fig. 3H), confirming that the mutations prevented TOCA-1 function, even though there was some remaining localisation to filopodia tips. Together, these results show that TOCA-1 function in filopodia is specific and dependent on a functional SH3 domain.

Cdc42 inhibition with CASIN reduces TOCA-1 and Ena at filopodia tips

To test whether TOCA-1 is specifically recruited to actively protruding filopodia and contributes to filopodial protrusion downstream of Cdc42, we treated RGCs with CASIN, a small molecule inhibitor of Cdc42 that acts rapidly and reversibly at concentrations up to 20 µM, but does not bind to other Rho GTPases, while an inactive CASIN analogue has no effect on Cdc42 (Peterson et al. 2006; Florian et al. 2012; Liu et al. 2019). CASIN suppresses adhesion and migration of Cdc42-wild type haematopoietic progenitor cells as strongly as a Cdc42 knockout, and CASIN treatment of Cdc42 knockout cells has no additional effect demonstrating the specificity of this reagent (Liu et al. 2019).

We reasoned that acute inhibition of Cdc42 should interfere with filopodial protrusion, and that if TOCA-1 is involved in filopodial protrusion via its HR1 domain interaction with Cdc42, TOCA-1 localisation would be disrupted. Time lapse videos of growth cones showed that acute inhibition of Cdc42 led to arrest of filopodial and lamellipodial dynamics (Fig. 4A, Movie 4), with only a mild reduction in filopodia numbers (Fig. 4B). CASIN treatment strongly limited initiation of new filopodia in a dose-responsive manner (Fig. 4C) and led to almost complete stalling of existing filopodia tips after 20 minutes of treatment (Fig. 4D). Loss of TOCA-1 at filopodia tips was associated with cessation of tip protrusion (Fig. 4E). After CASIN treatment (*right)* TOCA-1 is present up to the start of the last protrusion cycle, but no further cycles of protrusion were possible after loss of TOCA-1, whereas TOCA-1 puncta were often still present when filopodia tips stalled after DMSO treatment (*left*). Growth cones expressing Ena showed a similar pattern (Fig. 4F). Most growth cones still had tip fluorescence after 20 minutes of DMSO treatment (Fig. 4G), but after treatment with high concentration of CASIN, this dropped sharply for both mNG-TOCA-1 and mNG-Ena expressing growth cones. This confirms that both TOCA-1 and Ena are specifically recruited to protruding filopodia and respond to Cdc42-related changes in filopodial activity.

Journal of Cell Science • Accepted manuscript

A transient interaction of TOCA-1 and Ena in filopodial initiation

TOCA-1 and Ena display a clustering-dependent interaction *in vitro*, display similar dynamics in filopodia and response to Cdc42 inhibition, and partly overlap in filopodia. Two-colour single molecule localisation microscopy offers an opportunity to examine protein-specific ultrastructure and co-localisation at ~50 nm resolution, so we combined expression of mEos-Ena and photoactivated localisation microscopy (PALM) with immuno-staining of TOCA-1 and stochastic optical reconstruction microscopy (STORM) using Alexa Fluor-647-anti-rabbit secondary antibodies. Combined PALM/STORM resolves filopodia tips at high resolution, confirming that Ena and TOCA-1 are directly juxtaposed at a portion of filopodia tips (Fig. 5A, i-iii).

We reasoned that two-colour dynamic imaging would allow us to test whether the partial co-localisation of Ena and TOCA-1 seen in fixed cells corresponds to a transient event that is nonetheless predictive of filopodial extension. We expressed mNG-TOCA-1 with mScarlet-Ena in RGCs and developed a manual analysis pipeline (that does not require filopodia boundaries to be marked in the second channel) to study whether TOCA-1 and Ena coincide during filopodial initiation and extension. TOCA-1 and Ena frequently co-localised during filopodial initiation, and when filopodia resumed extension after stalling (Fig. 5B, Movie 5). At any given timepoint, 46% of filopodia had both TOCA-1 and Ena (mean of 3 frames, from 15 growth cones with 72 filopodia on average, with TOCA-1 and Ena each present in 60% and 63% of filopodia respectively). 57 of 202 filopodia underwent protrusion (initiation or re-extension) events during the videos. For each filopodium protrusion event, we tracked the filopodia tip and measured the intensity of mNG-TOCA-1 and mScarlet-Ena at the tip. We identified areas of TOCA-1/Ena overlap by setting an intensity threshold for each channel and selecting all areas with both proteins present with a minimum area of 0.06 μm^2 (approx. 14 pixels, to avoid single pixel fluctuations) and maximum of 1 μm^2 (orange regions in panel ii in Fig. 5C,E). The presence or absence of overlap at the tip was plotted relative to tip velocity during filopodial initiation and re-extension (Fig. 5D, F).

During filopodial initiation (Fig. 5B, annotated I, and Fig. 5C), we tracked the movement and fluorescence at the predicted base (the nearest region on the membrane to where the filopodium will form) before filopodial initiation, then at the tip after initiation. Both TOCA-1

Journal of Cell Science • Accepted manuscript

and Ena were abundant at the site of formation before protrusion, and typically both were present at the nascent filopodium tip, but after a few seconds one or both (especially TOCA-1) faded from the tip. To take one example, TOCA-1 and Ena overlap before initiation (-15 to 0 s), but overlap is only sometimes present after initiation (Fig. 5C). This same pattern was observed when pooling multiple examples (Fig. 5D). Overlap of TOCA-1 and Ena at the predicted base was observed in ~70% of initiating filopodia at all timepoints during the 30 s before initiation (Fig. 5D). After initiation, the proportion of filopodia tips with TOCA-1 and Ena overlap steadily falls to ~30%, suggesting that the TOCA-1/Ena complex forms transiently at the plasma membrane around the moment of filopodial protrusion.

Filopodial re-extension events were most often preceded by an advancing lamellipodium catching up with a static filopodium tip (17/32 events, annotated L, Fig. 5B panel ii and 5C), or otherwise often due to the merging of a second filopodium (11/32 cases), usually starting with the second tip contacting the first shaft (Fig. 5B panel i, annotated M). Frequently, one or both proteins (especially mNG-TOCA-1) were absent from the static tip before re-extension (Fig. 5E), and was provided by the joining lamellipodium or filopodium. For both TOCA-1 and Ena, peak fluorescence occurred just before re-extension, followed by a drop in tip fluorescence, especially for TOCA-1 (Fig. 5E, panel iii). Across 32 filopodia re-extension events, the resumption of filopodium tip protrusion coincided with a rapid increase in the proportion of filopodia tips with TOCA-1-Ena overlap, from less than 40% of filopodia -30 to -8s before re-extension, to around 75% of filopodia at the moment of re-extension, steadily falling to 50% around 30 s after (Fig. 5F; orange line). The increase in filopodia with TOCA-1/Ena overlap precedes the increase in mean tip velocity (Fig. 5F; black line), suggesting that a transient TOCA-1/Ena complex is associated with re-starting filopodial extension at mature tips. Together, our observations support a model in which TOCA-1 and Ena transiently associate before and during filopodia initiation and during re-extension.

Discussion

High spatial and temporal imaging of actin regulators alongside lamellipodial and filopodial dynamics gives valuable information about how cell players that are involved at multiple cellular sites, with multiple roles, are carrying out each function. In this work we have

Journal of Cell Science • Accepted manuscript

utilised quantitative analysis of fluctuations in protein recruitment to show that TOCA-1 localisation to filopodia has a functional role in filopodial protrusion, which we validated through statistical tests of causality and by mutagenesis and perturbation of TOCA-1 binding to Cdc42 and its interaction partners through the SH3 domain. We show that Ena is a functional interaction partner of TOCA-1, and we propose that TOCA-1 and Ena can form a regulatory complex at filopodia that transiently occurs before and during filopodium initiation and re-extension and stimulates protrusion. Our results complement and extend previous biochemical and perturbation studies which showed that TOCA-1 and paralogues are involved in filopodial formation though gave a conflicting picture of whether it promotes or opposes protrusion formation (Ho et al. 2004; Bu et al. 2009; Hu et al. 2011; Saengsawang et al. 2012; Taylor et al. 2019). Our strategy of quantitative dynamic analysis allowed us to show that TOCA-1 causes filopodial protrusion and promotes tip persistence.

When there are complex and nonlinear responses to perturbation of actin regulatory proteins (Skruber et al. 2020; Dimchev et al. 2021; Pokrant et al. 2023), multiple, complementary approaches are needed with different strengths, such as careful acute or inducible perturbations (Ghosh et al. 2004; Koestler et al. 2013), which limit system adaptation though still move the system far from physiological levels of target protein, and quantitative fluctuation analysis that allows investigation in a near-native setting. While our experiments were conducted by exogenous expression of TOCA-1, we showed there was no significant disruption of filopodial dynamics due to the mNG tag or overexpression under these conditions.

A role for TOCA-1 independent of membrane curvature sensing

TOCA-1 and other F-BAR proteins have well-described roles in endocytosis and promotion of positively curved membrane structures such as cytoplasmic tubular networks (Frost et al. 2008; Taylor et al. 2019; Ledoux et al. 2023), but there are precedents for these and related BAR proteins acting in negatively curved membrane structures (Qualmann & Kelly 2000; She et al. 2002; Chitu et al. 2005; Guerrier et al. 2009; Shimada et al. 2010; Becalska et al. 2013; Zhai et al. 2022). This suggests that any membrane curvature preference of F-BAR proteins does not limit them to certain cellular functions. This could be possible because of alternative binding modes that target flat membrane (Frost et al. 2008; McDonald et al.

Journal of Cell Science • Accepted manuscript

2015), or the presence of complex membrane curvatures in filopodia, for example those observed by EM in dendritic filopodial precursors (Galic et al. 2014) and described theoretically (Mancinelli et al. 2021), although we could not detect them in our single molecular localisation microscopy images. Membrane fluctuations, producing both positive and negative curvature, are proposed to recruit diverse BAR superfamily proteins with either curvature preference (Mattila et al. 2007; Mancinelli et al. 2021).

TOCA-1 and other membrane adaptor proteins in filopodial formation

While in cortical neurons colocalization of CIP4 with Mena to actin ribs has been seen, our analysis of filopodia provides correlative and quantitative insight into the influence of TOCA-1 on filopodia and its cooperation with Ena in Cdc42 driven rather than Rac1 driven events (Hu et al. 2011; Saengsawang et al. 2012, 2013). As well as F-BAR protein paralogues, lamellipodin (Krause et al. 2004), IRSp53 (Disanza et al. 2013), and recently formin FMNL2 (Fox et al. 2022), have been shown to play comparable membrane adaptor roles to TOCA-1 by scaffolding Ena, VASP or other actin regulators. The variety of these different contributors may reflect the different filopodia being studied, alternative mechanistic pathways, signalling-dependent use of adaptors or redundancy.

IRSp53 appears to localise to filopodia tips and shafts (Nakagawa et al. 2003; Sudhaharan et al. 2019; Cheng & Mullins 2020; Tsai et al. 2022). In contrast, TOCA-1 localises to discrete puncta, especially at filopodia tips. The multiple shaft puncta observed by immunostaining of endogenous TOCA-1 may correspond to the dynamic puncta moving up and down shafts observed in videos of mNG-TOCA-1, or a pool of TOCA-1 not labelled by mNG-TOCA-1. Live imaging shows that puncta of TOCA-1 mostly localise to tips or transiently during initiation/re-extension events, suggesting a specific role distinct from the more structural role of I-BAR proteins in stabilising curved filopodial membrane.

Similar to clusters of lamellipodin (Cheng & Mullins 2020), TOCA-1 is first recruited to plasma membrane, then moves laterally and coalesces into larger puncta that recruit Ena and sometimes develop into filopodia. Furthermore, the frequent observation of TOCA-1 puncta moving inwardly, often associated with filopodial formation, is consistent with size-dependent splitting of the TOCA-1 cluster to maintain appropriate stoichiometry, as

Journal of Cell Science • Accepted manuscript

observed for the lamellipodin-VASP complex (Cheng & Mullins 2020), though other explanations are possible such as coincident retrograde movement of a membrane vesicle (Nozumi et al. 2017; Gallop 2020). Fixed imaging did not capture a consistent arrangement of TOCA-1 and Ena, even at super-resolution, though rapid, time-resolved super-resolution imaging could be useful in revealing any arrangement of the transient TOCA-1/Ena complex during filopodial protrusion and how it links to the membrane.

The mechanisms of TOCA-1 promoting filopodial protrusion

Though TOCA-1 and Ena interact directly *in vitro* they did not persistently co-localise in cells, suggesting that specific conditions are needed for their interaction, and we provide evidence that a sufficient density of TOCA-1 is a key factor. The proportion of filopodia tips with TOCA-1 and Ena overlap was substantially higher before and during filopodium initiation and re-extension compared to static tips. Measuring the degree of overlap is a simplification to capture and quantify the coincidence of the two proteins, quantifying the fluorescence intensity of each protein is consistent with a transient peak in abundance associated with dynamic filopodia events. Use of Split-GFP may prove helpful in future studies to monitor the direct interaction in cells.

As well as filopodial extension, TOCA-1 appears to have a particular role in filopodial initiation, since it arrives before Ena at sites of filopodial initiation, and TOCA-1/Ena overlap is more abundant at the tips of short (potentially young) filopodia. N-WASP, an activator of Arp2/3 complex and branched actin, binds TOCA-1 at both high and low densities. It is possible that when TOCA-1 is initially recruited to leading edge membranes, at lower density, it promotes polymerisation of branched actin structures via N-WASP or WAVE, such as advancing lamellipodia (Ho et al. 2004; Fricke et al. 2009). Then, after attaining sufficiently high density by coalescence of multiple puncta, TOCA-1 may switch to promoting linear actin polymerisation via Ena and formins, leading to filopodial initiation or re-extension. The clustering of TOCA-1 required for Ena binding is similar to observations with VASP clustered on beads (Breitsprecher et al. 2008) and the increased processivity similar to the activity of Ena on filaments clustered by fascin (Harker et al. 2019). TOCA-1 responding filopodia had strongly increased persistence of tip movement, suggesting TOCA-1 promotes

Journal of Cell Science • Accepted manuscript

filopodia that are resistant to interruptions in protrusion, perhaps by contributing to the assembly of a robust complex of actin regulators including Ena at the filopodia tip.

Our results reiterated previous findings in neuronal cells that TOCA-1 mutants lacking an intact SH3 domain lost their function (Bu et al. 2009; Saengsawang et al. 2012) while in epithelioid cells the recruitment of TOCA-1 to EGF-stimulated filopodia was not reliant on the SH3 domain (Hu et al. 2011). The mutants still had some filopodial localisation, with cross-correlation and GCA confirming their loss of function, demonstrating the power of these approaches. The remaining localisation still present is likely due to heterodimerisation with endogenous TOCA-1, as the mutants also caused a dominant negative effect, thus supporting a role for clustered TOCA-1 in filopodial growth.

Further work is needed to explore the possible interplay between the TOCA-1/N-WASP/WAVE and TOCA-1/Ena complexes, confirming if they are spatially and temporally separated, and dissecting the relationship between advancing lamellipodia and protruding filopodia. Quantitative image analysis approaches build on the candidate list of filopodial regulators characterised by biochemical, genetic and chemical perturbation studies. They offer the opportunity to untangle these processes and compare the multiple roles for shared actin regulators at different cellular sites *in vivo* without widespread alterations in the regulatory balance of actin architecture.

Materials and Methods

Plasmids

pET-His-SNAP-TOCA-1 (*Xenopus tropicalis*; BC080964), pCS2-His-SNAP-Ena (*X. laevis*; BC073107) and pET-KCK-VASP (*X. laevis*; BC077932), or SNAP alone, were generated previously (Dobramysl et al. 2021). mNeonGreen was supplied by Allele Biotechnology and Pharmaceuticals (Shaner et al. 2013) and pCS2-mNG-Ena and pCS2-mNG alone were generated previously (Urbančič et al. 2017). New vectors were generated by PCR (Phusion-HF, NEB) into parent vectors digested with FseI/AscI unless otherwise stated. pCS2-mNG-TOCA-1 was generated by sub-cloning TOCA-1 into the digested pCS2-mNG vector, with oligonucleotide primers: 5'-GCATGGCCGGCCACCATGAGCTGGGGTACTG-3' and 5'-

Journal of Cell Science • Accepted manuscript

GGCGCGCCTTAGATATAAGTTACTGC-3'. Ena was subcloned using primers: 5'-GCATGGCCGGCCACCATGAGTGAACAGAGCATC-3' and 5'-GGCGCGCCCTATGCGCTGTTTG-3' into pCS2 vectors generated with mEos3.2 (amplified from pmEos3.2-N1, which was a gift from Michael Davidson & Tao Xu (Zhang et al. 2012); Addgene plasmid 54525) or mScarlet (amplified from pLifeAct_mScarlet_N1, which was a gift from Dorus Gadella (Bindels et al. 2017); Addgene 85054). GAP43-RFP was a gift from the Holt laboratory. A version of His-Ena without SNAP was generated using the above Ena primers. Ena-ΔPRR was generated by replacement of S291-G373 with a linker sequence GGGGSSGG, using In-Fusion cloning (Takara Bio) with primer pairs: 5'-TCATCATCACGAATTCAGGCCGGCC-3' + 5'-ACCTGAAGAACCACCTCCTCCCACTCTCCGTTCCCTTTCCCATTCC-3' and 5'-GGTGGTTCTTCAGGTGGATCAGAAGAGAATCGTGCTTTATC-3' + 5'-GGCCGCGGCGCCAATGCATTGGGCC-3' into the parent vector digested with EcoRI and NotI. VASP-ΔPRR was generated by removal of S116-S192, using In-Fusion cloning with primer pairs: 5'-ACAATTCCCCTCTAGAAATAATTTTG-3' + 5'-CACCCCCACCAGTCTCCAGTGCATCCAAGG-3' and 5'-AGACTGGTGGGGGTGGAGGAAGCTCAGGTGG-3' + 5'-TATCATCGATAAGCTTTAATGCGGTAG -3' into the parent vector digested with HindIII and XbaI. The additional mutation in construct M1 (P234G) was generated by PCR (Pwo Master; Roche) using primers: 5'-CCTCCCCAGTTGGTGGAGTGGGTGCAAAGCCAGACATAAGTCG-3' and 5'-CGACTTATGTCTGGCTTTGCACCCACTCCACCAACTGGGGAGG-3'. TOCA-1 mutants were generated as shown in Fig. 3A. For mutants starting at the N-terminus, the forward primer was 5'-GCATGGCCGGCCACCATGAGCTGGGGTACTG-3' and the reverse primers were 5'-GGCGCGCCTTAGCTGTAGTCTTCAAAGGGATAGTC-3' (FBAR only), 5'-GGCGCGCCTTATTGTGCTACAAGATGGTTAGCTTC-3' (FBAR-HR1) and 5'-GGCGCGCCTTAAGCTGGGAGAGGTTCATCATC-3' (FBAR-HR-linker). The SH3 only mutant was generated using primers: 5'-GCATGGCCGGCCACCATGGGACACTGCAAATCAC-3' and 5'-GGCGCGCCTTATAGAGTGATATCTATGTAGGATGTGG-3' and the W517K mutant was generated using primers: 5'-GATAAAGGGGATGGAAAGACAAGAGCAAG-3' and 5'-CTTGCTCTTGTCTTTCCATCCCCTTTATC-3'. Human TOCA-1 was sub-cloned into the pCS2-mNG vector using primers 5'-GATCGGCCGGCCATGAGCTGGGGCACGGAGC-3' and 5'-GGCGCGCCCTGCAGCTCGAGTCAGGAACC-3'.

Journal of Cell Science • Accepted manuscript

Protein expression and purification

His-tagged proteins were expressed and purified with Ni-NTA columns and gel filtration on S200 columns as previously (Dobramysl et al. 2021) with some exceptions. His-SNAP-TOCA-1 was purified in high salt buffers (300 mM NaCl instead of 150 mM NaCl during washing and elution), with two additional washes with 50 mM imidazole elution buffer before elution in a single 300 mM imidazole step and concentration using a spin concentrator before proceeding to gel filtration. TOCA-1 mutants were expressed and purified in the same way as wild type TOCA-1. His-Ena-ΔPRR was expressed in 293F cells and purified in the same way as wild type Ena (Dobramysl et al. 2021), except that 300 mM NaCl, not 150 mM, was used in wash and elution buffers. His-KCK-VASP mutants were expressed in BL21 *E. coli* in the same way as Ena mutants. His-SNAP alone was purified with elutions at 100 mM and 300 mM imidazole.

Coupling to beads, including densities, and precipitation from HSS

For each reaction, 20-40 µl SNAP-Capture beads (NEB, S9145S) were pre-equilibrated in 150 mM NaCl, 20 mM HEPES (pH 7.4), 0.1% TWEEN-20, then 500 µl of SNAP-coupled protein was added overnight, under rotation at 4°C in buffer containing 150 mM NaCl, 20 mM HEPES (pH 7.4), 0.1% TWEEN-20 and 1 mM DTT. Beads were washed five times in 150 mM NaCl, 50 mM Tris, 1 mM DTT, 0.1% TWEEN-20. The capacity of benzylguanine sites on beads was determined empirically for each protein, with, per 40 µl of beads, 500 µl of 12 µM SNAP-TOCA-1 or mutants; 500 µl of 24 µM SNAP alone. For varying the density of TOCA-1 on beads, 500 µl of 2 µM SNAP-TOCA-1 was coupled to 10 µl of beads (determined to be maximum capacity) or 50 µl (intermediate density) or 100 µl (low density), then, respectively, 90 µl, 50 µl or 0 µl of un-coupled beads were added to make a final volume of 100 µl beads for each condition, and a control sample with 100 µl un-coupled beads was also prepared. In a second stage of coupling, 500 µl of 80 µM SNAP alone was then added, to bind the remaining benzylguanine sites on the beads. To precipitate proteins from *Xenopus* HSS, coupled beads were incubated for 1 h at 4°C with 400 µl *Xenopus* HSS (prepared as previously described (Walrant et al. 2015) and diluted to 4.17 mg/ml in 50 mM Tris, 150 mM NaCl, 2 mM DTT and energy mix [50 mM phosphocreatine, 20 mM Mg-ATP (adjusted to pH 7.0 with Tris base), 20 mM $MgCl_2$]). To precipitate purified Ena/VASP, 100 µl of 1 µM protein was incubated with 10 µl of coupled beads.

Journal of Cell Science • Accepted manuscript

Antibody affinity purification

Affi-Gel 15 beads (Bio-Rad, 1536051) were equilibrated in 300 mM NaCl, 20 mM Na-HEPES pH 7.4, 2 mM EDTA and 2 mM DTT, then incubated with His-SNAP-TOCA-1, or SNAP alone, for 4 h, 4˚C under rotation. 1 M mono-ethanolamine pH 8 was added to block (1 h), then the TOCA-1-coupled beads were washed on a column with the following buffers: 500 mM NaCl and 20 mM Na-HEPES, glycine-HCl pH 2.5, tri-ethylamine pH 11.5. The harvest bleed serum was passed through the column coupled to SNAP alone, then the flow through applied to the column coupled to His-SNAP-TOCA-1 (2 h, room temperature, under rotation). The column was washed in 20 ml of 400 mM NaCl, 30 mM Na-HEPES pH 7.7 and 3 ml of 300 mM NaCl, 10 mM Tris-HCl pH 7.2, before elution. Elution with acid was carried out with 100 mM glycine pH 2.5, 300 mM NaCl and neutralised in 1.5 M Tris-HCl pH 8.8, followed by elution with base using 100 mM triethylamine pH 11.5, 300 mM NaCl and neutralisation in 2 M Tris-HCl pH 6.5. Elution fractions were screened by absorbance at 280 nm and pooled, before exchanging buffer to 10 mM K-HEPES, 100 mM KCl, 1 mM $MgCl_2$, 100 nM $CaCl_2$, pH 7.4 overnight.

Western blotting and antibodies

Samples for western blotting were separated on 4-20% gradient polyacrylamide gels (Mini-PROTEAN TGX, Bio-Rad, 456-1096) and transferred to nitrocellulose membranes by wet transfer in 25 mM Tris, 192 mM glycine, 0.1% SDS, 20% methanol for 1 h at 0.38 A (Bio-Rad Mini Trans-Blot Cell apparatus) or dry transfer (programme 0, iBlot 2, ThermoFisher). Membranes were blocked in 5% milk powder/0.1% TWEEN-20/Tris-buffered saline (20-60 minutes, room temperature) and stained with primary antibody in blocking solution (1 h at room temperature or 4˚C overnight). Membranes were washed 3-5 times in 0.5% milk powder/0.1% TWEEN-20/Tris-buffered saline for 5-10 minutes then incubated with goat anti-rabbit 800CW secondary antibody (Li-Cor, 926-32211; 30-60 minutes, room temperature) before washing as before and imaging on a LI-COR BioSciences Odyssey Sa scanner. For testing density dependence, three replicate blots were quantified using LI-COR Unicorn software, with a Friedman test to assess differences across the unclustered, intermediate and clustered states.

Journal of Cell Science • Accepted manuscript

Antibodies for blotting: affinity purified anti-TOCA-1 antibody (described above) or other unpurified bleeds (1:500 dilution). The anti-Ena (1:15000), anti-VASP (1:500) and anti-N-WASP (1:2000) antibodies were affinity purified and described previously (Dobramysl et al. 2021), as was the anti-Diaph3 antibody (1:1300), a gift from Marc Kirschner (Ho et al. 2004). Antibodies for immunostaining cells: affinity purified anti-TOCA-1 antibody (described above; 1:500 dilution). Secondary antibodies used for immunostaining: goat anti-rabbit-AlexaFluor 488 (1:2000, Invitrogen, A11008), goat anti-rabbit-AlexaFluor 647 (1:2000, Invitrogen, A21244). For images of uncropped blots see Fig. S5.

RGC preparation and injection of RNA

This research was regulated under the Animals (Scientific Procedures) Act 1986 Amendment Regulations 2012 following ethical review by the University of Cambridge Animal Welfare and Ethical Review Body. *Xenopus* embryos were fertilised *in vitro*, RNA was introduced by electroporation at stages 26-28 and RGC explants were taken at stages 35-36 and cultured for 19-24 h in 60% L-15 (Sigma-Aldrich, L1518) in water, on 35 mm glass-bottom dishes (MatTek P35G-1.5-14-C) coated with 10 µg/ml poly-L-lysine for 1 h (Sigma, P8920) and 10 µg/ml laminin for 5-10 minutes (Sigma, L2020) as described previously (Falk et al. 2007; Leung & Holt 2008; Urbančič et al. 2017). For experiments with CASIN treatment, mScarlet-Ena, mEos-Ena or for immunostaining, 75 pg of RNA was micro-injected into the neural fated blastomeres of 4 cell embryo instead of electroporation. mNG-TOCA-1 and mScarlet-Ena were co-injected at a ratio of 1:2 to equalise the resultant fluorescence levels. Capped RNA was synthesised after linearisation with NotI using SP6 mMessage mMachine kit (Invitrogen, AM1340) with elution into RNase-free water.

Live imaging of RGCs

Live imaging of RGCs was conducted in 60% L-15/water under HILO illumination on a custom made TIRF setup described previously (Urbančič et al. 2017) with an iLas2 illuminator (Roper Scientific), an Optosplit beam splitter (Cairn Research) and a CMOS camera (Hamamatsu ORCA-Flash4.0). Imaging of TOCA-1 mutants and experiments with CASIN treatment were acquired on a similar setup modified with a Multisplit beam splitter (Cairn Research) and a Kinetix CMOS camera (Photometrics) used in 12-bit (sensitivity) mode. Images were acquired at a rate of 2 s per time point (mNG-TOCA-1/GAP43-RFP videos), 7.5 s per time

Journal of Cell Science • Accepted manuscript

point (CASIN treatment videos) or else 1.5 s per time point, with a 100x 1.49 NA oil immersion objective (pixel size 0.065 µm) at room temperature, controlled by MetaMorph software (Molecular Devices). Where drugs were added, DMSO, or CASIN (S6875, Stratech Scientific) dissolved in DMSO were diluted in 1:500 in 60% L-15/water to make a 2x solution. After 5 minutes of imaging (before drug), acquisition was paused, half the ~ 350 µl RGC media was removed and replaced with the same volume of 2x drug solution, for a final DMSO concentration of 0.1%. The process of addition typically took 1-2 minutes, before acquisition was resumed.

Fixed imaging of RGCs and PALM/STORM

RGCs were washed once in 60% L-15/water then fixed in 4% PFA/7.5% sucrose/PBS (0.5 – 1 h, room temperature) and washed three times in 0.002% Triton X-100/PBS. Cells were permeabilised in 0.1% Triton X-100/PBS (3 minutes, room temperature) then washed twice as before and blocked in 5% goat serum/0.002% Triton X-100/PBS (overnight, 4˚C). Primary antibody was diluted in blocking solution and added to cells (1 h, room temperature) with three washes in 0.5% goat serum/0.002% Triton X-100/PBS (5 minutes each). Secondary antibody was diluted in blocking solution and added to cells (30 minutes, room temperature) with phalloidin-AlexaFluor568 (1:100 dilution, Invitrogen, A12380) included when indicated, before washing as before. Cells were imaged in wash buffer by TIRF (as for live imaging), or for TOCA-1/GAP43 image (Fig. 1D) and Fig. S2C, imaged with a Photometrics Evolve Delta EM-CCD camera instead.

For PALM/STORM imaging, wash buffer was replaced with 150 µl STORM buffer (enzyme mix (50 µg/ml catalase (Sigma), 50 mM Tris-HCl (pH 7.5), 0.5 mg/ml glucose oxidase (Sigma)), 100 mg/ml D-Glucose (Sigma)/ddH_2O, 100 mM cysteamine hydrochloride (MEA, Sigma, M6500)/ddH_2O), and dishes were sealed by lowering a coverslip (18 x 18 mm) onto the central well. Images were acquired on an N-STORM system controlled by NIS Elements AR version 4.50, with an Agilent laser bed (405 nm, 488 nm, 561 nm, 647 nm lasers), CPI Plan Apo 100x 1.49 NA objective and an N-STORM QUAD filter (405/488/561/647), and imaging with an iXon Ultra 897 EM-CCD camera (Andor). PALM/STORM images were acquired sequentially, in TIRF, with around 10,000 frames (20 ms) of PALM imaging (using low laser power (1-10%) 405 nm to sparsely photoconvert mEos and 561 nm laser at high

Journal of Cell Science • Accepted manuscript

laser power for imaging) followed by 20,000-30,000 frames (20 ms) of STORM imaging (using low laser power 405 nm to tune blinking rates and 1-2 kW/cm^2 647 nm illumination). TIRF reference images (Fig. 5A) were acquired using the same system.

Image processing and analysis

Image processing was performed in FIJI (Schindelin et al. 2012) with custom macros for analysis and some processing macros developed by Steve Rothery at the FILM facility, Imperial College London (www.imperial.ac.uk/medicine/facility-for-imaging-by-light-microscopy/software/fiji/). Images were processed by overlaying the two channels (when Optosplit used) and de-noising with nd-safir (for Fig. 2B, Movie 2) (Boulanger et al. 2010) or a 50-70 px rolling ball background subtraction for all other images. Videos with CASIN treatment were registered using Fast4DReg (without time averaging) to remove stage drift (Laine et al. 2019; Pylvänäinen et al. 2023).

For quantifying the prevalence of TOCA-1 or Ena in fixed or live images of filopodia, all filopodia protruding from the growth cone (not the axon) of length ≥3 µm were counted and scored visually for the presence of TOCA-1 or Ena in the filopodia shaft or tip. For quantifying TOCA-1/Ena overlap in filopodia from immunostained RGCs, individual filopodia of length ≥3 µm were extracted using the rotated rectangle tool, then measured using a straight line from tip (defined by GAP43-RFP where present, else by the furthest punctum of Ena or TOCA-1 in line with the shaft) to base (defined as the start of a region of consistent, narrow width). Puncta were counted automatically, after manual thresholding to exclude most of the noise, as particles between 0.06 (corresponding to around 14 pixels, or a box of sides 250 nm) – 1.00 µm^2. Overlap puncta were identified using a binary addition of the two thresholded images, and again automatically selecting resultant overlap puncta with area 0.06 – 1.00 µm^2. Tip localised puncta were defined as being at least half within a 1 µm circle anchored to the tip. Significance was assessed with a Student's t-test, if normally distributed according to a Jarque-Bera test, or a Kruskal-Wallis test if not.

Videos of mNG-TOCA-1 or mNG-Ena and GAP43-RFP-expressing RGCs were analysed with Filopodyan (Urbančič et al. 2017) (without de-noising), using thresholding parameters: RenyiEntropy / Fit tip / ED iterations 4 / LoG sigma 2.6-3.6, or other parameters that best

Journal of Cell Science • Accepted manuscript

segmented each video; and filter settings: Min start frame: 1 / Min frames: 3 / Min max length: 1.8 / Min length change: 0.1 / Max mean waviness: 0.38. Tracks assigned to filopodia that merged, moved out of focus or were otherwise poorly annotated were manually excluded.

Data tables were then analysed using FilopodyanR, with fluorescence signal processed by background subtraction based on signal near the growth cone boundary, then normalisation to growth cone body fluorescence. For plotting base fluorescence, the normalised time series were detrended by removing a linear trend, then mean base fluorescence at the predicted base plotted, with a moving average (window size 5). Tip movement data was processed by removal of outliers (top and bottom 0.5%) then smoothing with a moving average with window size of 3, or for CASIN treated data, a window size of 5 and removal of top and bottom 1% outliers (Urbančič et al. 2017). CCF scores were calculated and plotted using the "FilopodyanR CCF.R" script, with time series filtered by minimum 50 frames. Missing values were not removed during CCF calculation.

Kymographs of TOCA-1/Ena fluorescence were generated using the Filopodyan "Process Profile Graphs" option, plotting the segmented filopodium base, shaft and tip as a straight line for each frame. The camera offset was subtracted from the raw fluorescence values, then the fluorescence values were normalised by the median fluorescence intensity in the growth cone body, to account for varying expression levels in different cells. Low contrast images of the kymograph were used to mark the filopodium outline.

Videos of RGCs treated with CASIN were scored visually, comparing before (-5 to 0 minutes) and after (15-20 minutes) DMSO/drug treatment, for the presence of one or more filopodia with a sustained, clear punctum of tip fluorescence. Data show mean of two independent, blinded assessments. Temporal projections were prepared using the Temporal-Color Code plugin in Fiji.

TOCA-1 puncta behaviour was quantified from mNG-TOCA-1/GAP43-RFP videos after de-noising. For scoring of numbers of coalescing puncta used the maximum number of distinct puncta that were observed during the < 14 s before filopodial initiation. For quantifying the

Journal of Cell Science • Accepted manuscript

fate of TOCA-1 puncta, a macro was used to track all puncta with minimum 5 frames, minimum 0.65 µm link distance and starting within 1 µm of the leading edge. Then individual puncta were randomly selected from a list to then be manually assigned to a category.

Videos of mNG-TOCA-1 and mSc-Ena were processed manually, with background subtraction, extraction of filopodia that underwent initiation or re-extension events using a rotated rectangle to re-orientate parallel to the long axis of the filopodium. Fluorescence intensity values were extracted along the length of the filopodium (averaging across a ~20 px column for each pixel along the long axis) using a line profile tool (line/time macro; FILM facility). Overlap puncta were defined as areas of overlap 0.06 – 1.00 μm^2 after thresholding and binary addition as for fixed images above, and scored as positive if any pixels in the ~20 pixel column were part of an overlap punctum. The tip was tracked manually using TrackMate (Tinevez et al. 2017), and a custom Excel worksheet was used to extract the fluorescence intensity values and presence or absence of any TOCA-1/Ena overlap at the filopodium tip (averaged over 5 pixel window centred on tip along the long axis of filopodium). The velocity was calculated as displacement along the long axis for each frame and velocity and fluorescence intensity values, and proportion with TOCA-1/Ena overlap, were smoothed by a moving average over 3 frames.

Granger Causality Analysis

GCA was conducted on the same processed time series used for cross-correlation analysis. To begin the analysis, the stationarity of our time series was confirmed via the Augmented Dickey Fuller test (Dickey & Fuller 1979). Next, we selected the optimum lag for the Granger Causality test by selecting the lag from 1 to 5 that minimized the Bayesian information criteria (Schwarz 1978). We tested Granger Causality using the MATLAB function gctest(). Raw p-values were corrected for multiple hypothesis testing using the Benjamini-Hochberg false discovery rate procedure (Benjamini & Hochberg 1995).

Super Resolution Image Reconstruction

Image data stacks were converted from Nikon image files into TIF stacks using Fiji. Single molecule blinking events were detected in unprocessed camera frames and fit with a two-

Journal of Cell Science • Accepted manuscript

dimensional (2D) gaussian model as previously described (Li et al. 2018). Fit results were filtered based on number of photons (50 - 5000), localisation precision (0.5 – 50 nm), goodness of fit (LLR < 150) and PSF width (sigma, 50 – 150 nm). Post processing drift correction was applied using a redundant cross-collection algorithm as previously described (Wang et al. 2014). Because PALM and STORM datasets were collected sequentially, in that order, drift correction was applied relative to the last frame of the PALM image and to the first frame of the STORM image. Images were reconstructed with a 16 nm pixel size and blurred with a 2D Gaussian equal to the image's average localisation precision.

Acknowledgements

We would like to thank Asha Dwivedy for help with eye primordia electroporation and dissection, Jonathan Gadsby for helping with affinity purification of the anti-TOCA-1 antibody and Marc Kirschner (Harvard Medical School) for supplying the anti-Diaph3 antibody.

Author contributions

Conceptualization: H.M.F., V.U., J.L.G.; Methodology: T.C.A.B., A.W., J.M.; Software: T.C.A.B., V.U., R.R.; Validation: T.C.A.B., J.M.; Formal analysis: T.C.A.B., V.U., E.S.A., R.R.; Investigation: T.C.A.B., H.M.F., V.U., A.W., J.M.; Data curation: T.C.A.B., V.U.; Writing – original draft: T.C.A.B., J.L.G.; Writing – review and editing: H.M.F., V.U., A.W., J.M., E.S.A., T.C.A.B., J.L.G.; Visualization: T.C.A.B., H.M.F.; Supervision: J.L.G. and G.D.; Project administration: J.L.G.; Funding acquisition: J.L.G. and G.D.

Funding

This work was supported by Wellcome Trust Research Career Development Fellowship WT095829MA and Senior Research Fellowship 219482/Z/19/Z to J.L.G. and studentship 099740/Z/12/Z to H.M.F.; A.W. was supported by a Biochemical Society Summer Vacation Studentship. We acknowledge core funding by the Wellcome Trust (092096) and Cancer Research UK (C6946/A14492), as well as NIGMS RM1GM145399 (UTSW-UNC Center for Cell Signaling Analysis).

Journal of Cell Science • Accepted manuscript

Data availability

Data and reagents are available on request to J.L.G.

Competing Interests

The authors declare no competing interests.

References

Applewhite DA, Barzik M, Kojima S, Svitkina TM, Gertler FB, Borisy GG. 2007. Ena/VASP Proteins Have an Anti-Capping Independent Function in Filopodia Formation. *Mol Biol Cell*. 18(7):2579–91

Barzik M, McClain LM, Gupton SL, Gertler FB. 2014. Ena/VASP regulates mDia2-initiated filopodial length, dynamics, and function. *Mol Biol Cell*. 25(17):2604–19

Bear JE, Svitkina TM, Krause M, Schafer DA, Loureiro JJ, et al. 2002. Antagonism between Ena/VASP Proteins and Actin Filament Capping Regulates Fibroblast Motility. *Cell*. 109(4):509–21

Becalska AN, Kelley CF, Berciu C, Stanishneva-Konovalova TB, Fu X, et al. 2013. Formation of membrane ridges and scallops by the F-BAR protein Nervous Wreck. *Mol Biol Cell*. 24(15):2406–18

Benjamini Y, Hochberg Y. 1995. Controlling the False Discovery Rate: A Practical and Powerful Approach to Multiple Testing. *J. R. Stat. Soc.: Ser. B (Methodol.)*. 57(1):289–300

Bindels DS, Haarbosch L, Weeren L van, Postma M, Wiese KE, et al. 2017. mScarlet: a bright monomeric red fluorescent protein for cellular imaging. *Nat Methods*. 14(1):53–56

Blake TCA, Gallop JL. 2023. Filopodia In Vitro and In Vivo. *Annu. Rev. Cell Dev. Biol.* 39(1):

Boulanger J, Kervrann C, Bouthemy P, Elbau P, Sibarita J-B, Salamero J. 2010. Patch-Based Nonlocal Functional for Denoising Fluorescence Microscopy Image Sequences. *Ieee T Med Imaging*. 29(2):442–54

Breitsprecher D, Kiesewetter AK, Linkner J, Urbanke C, Resch GP, et al. 2008. Clustering of VASP actively drives processive, WH2 domain-mediated actin filament elongation. *Embo J*. 27(22):2943–54

Bu W, Chou AM, Lim KB, Sudhaharan T, Ahmed S. 2009. The Toca-1-N-WASP Complex Links Filopodial Formation to Endocytosis. *J Biol Chem*. 284(17):11622–36

Journal of Cell Science • Accepted manuscript

Burke TA, Christensen JR, Barone E, Suarez C, Sirotkin V, Kovar DR. 2014. Homeostatic Actin Cytoskeleton Networks Are Regulated by Assembly Factor Competition for Monomers. *Curr. Biol.* 24(5):579–85

Chan CE, Odde DJ. 2008. Traction Dynamics of Filopodia on Compliant Substrates. *Science*. 322(5908):1687–91

Cheng KW, Mullins RD. 2020. Initiation and disassembly of filopodia tip complexes containing VASP and lamellipodin. *Mol Biol Cell*. 31(18):2021–34

Chitu V, Pixley FJ, Macaluso F, Larson DR, Condeelis J, et al. 2005. The PCH Family Member MAYP/PSTPIP2 Directly Regulates F-Actin Bundling and Enhances Filopodia Formation and Motility in Macrophages. *Mol Biol Cell*. 16(6):2947–59

Damiano-Guercio J, Kurzawa L, Mueller J, Dimchev G, Schaks M, et al. 2020. Loss of Ena/VASP interferes with lamellipodium architecture, motility and integrin-dependent adhesion. *Elife*. 9:e55351

Dickey DA, Fuller WA. 1979. Distribution of the Estimators for Autoregressive Time Series With a Unit Root. *J. Am. Stat. Assoc.* 74(366):427

Dimchev G, Steffen A, Kage F, Dimchev V, Pernier J, et al. 2017. Efficiency of lamellipodia protrusion is determined by the extent of cytosolic actin assembly. *Mol. Biol. Cell*. 28(10):1311–25

Dimchev V, Lahmann I, Koestler SA, Kage F, Dimchev G, et al. 2021. Induced Arp2/3 Complex Depletion Increases FMNL2/3 Formin Expression and Filopodia Formation. *Frontiers Cell Dev Biology*. 9:634708

Disanza A, Bisi S, Winterhoff M, Milanesi F, Ushakov DS, et al. 2013. CDC42 switches IRSp53 from inhibition of actin growth to elongation by clustering of VASP. *Embo J*. 32(20):2735–50

Dobramysl U, Jarsch IK, Inoue Y, Shimo H, Richier B, et al. 2021. Stochastic combinations of actin regulatory proteins are sufficient to drive filopodia formation. *J Cell Biology*. 220(4):e202003052

Dwivedy A, Gertler FB, Miller J, Holt CE, Lebrand C. 2007. Ena/VASP function in retinal axons is required for terminal arborization but not pathway navigation. *Development*. 134(11):2137–46

Falk J, Drinjakovic J, Leung KM, Dwivedy A, Regan AG, et al. 2007. Electroporation of cDNA/Morpholinos to targeted areas of embryonic CNS in Xenopus. *Bmc Dev Biol*. 7(1):107

Feng Y, Hartig SM, Bechill JE, Blanchard EG, Caudell E, Corey SJ. 2010. The Cdc42-interacting Protein-4 (CIP4) Gene Knock-out Mouse Reveals Delayed and Decreased Endocytosis*. *J. Biol. Chem.* 285(7):4348–54

Journal of Cell Science • Accepted manuscript

Florian MC, Dörr K, Niebel A, Daria D, Schrezenmeier H, et al. 2012. Cdc42 Activity Regulates Hematopoietic Stem Cell Aging and Rejuvenation. *Cell Stem Cell*. 10(5):520–30

Fox S, Tran A, Trinkle-Mulcahy L, Copeland JW. 2022. Cooperative assembly of filopodia by the formin FMNL2 and I-BAR domain protein IRTKS. *J Biol Chem*. 298(11):102512

Fricke R, Gohl C, Dharmalingam E, Grevelhörster A, Zahedi B, et al. 2009. Drosophila Cip4/Toca-1 Integrates Membrane Trafficking and Actin Dynamics through WASP and SCAR/WAVE. *Curr Biol*. 19(17):1429–37

Frost A, Perera R, Roux A, Spasov K, Destaing O, et al. 2008. Structural Basis of Membrane Invagination by F-BAR Domains. *Cell*. 132(5):807–17

Galic M, Tsai F-C, Collins SR, Matis M, Bandara S, Meyer T. 2014. Dynamic recruitment of the curvature-sensitive protein ArhGAP44 to nanoscale membrane deformations limits exploratory filopodia initiation in neurons. *Elife*. 3:e03116

Gallop JL. 2020. Filopodia and their links with membrane traffic and cell adhesion. *Semin Cell Dev Biol*. 102:81–89

Ghosh M, Song X, Mouneimne G, Sidani M, Lawrence DS, Condeelis JS. 2004. Cofilin Promotes Actin Polymerization and Defines the Direction of Cell Motility. *Science*. 304(5671):743–46

Giuliani C, Troglio F, Bai Z, Patel FB, Zucconi A, et al. 2009. Requirements for F-BAR Proteins TOCA-1 and TOCA-2 in Actin Dynamics and Membrane Trafficking during Caenorhabditis elegans Oocyte Growth and Embryonic Epidermal Morphogenesis. *PLoS Genet.* 5(10):e1000675

Gouder L, Vitrac A, Goubran-Botros H, Danckaert A, Tinevez J-Y, et al. 2019. Altered spinogenesis in iPSC-derived cortical neurons from patients with autism carrying de novo SHANK3 mutations. *Sci Rep-uk*. 9(1):94

Guerrier S, Coutinho-Budd J, Sassa T, Gresset A, Jordan NV, et al. 2009. The F-BAR Domain of srGAP2 Induces Membrane Protrusions Required for Neuronal Migration and Morphogenesis. *Cell*. 138(5):990–1004

Hansen SD, Mullins RD. 2015. Lamellipodin promotes actin assembly by clustering Ena/VASP proteins and tethering them to actin filaments. *eLife*. 4:e06585

Harker AJ, Katkar HH, Bidone TC, Aydin F, Voth GA, et al. 2019. Ena/VASP processive elongation is modulated by avidity on actin filaments bundled by the filopodia cross-linker fascin. *Mol Biol Cell*. 30(7):851–62

He K, Sakai T, Tsukasaki Y, Watanabe TM, Ikebe M. 2017. Myosin X is recruited to nascent focal adhesions at the leading edge and induces multi-cycle filopodial elongation. *Sci Rep-uk*. 7(1):13685

Journal of Cell Science • Accepted manuscript

Ho H-YH, Rohatgi R, Lebensohn AM, Ma L, Li J, et al. 2004. Toca-1 Mediates Cdc42-Dependent Actin Nucleation by Activating the N-WASP-WIP Complex. *Cell*. 118(2):203–16

Hu H-T, Shih P-Y, Shih Y-T, Hsueh Y-P. 2016. The Involvement of Neuron-Specific Factors in Dendritic Spinogenesis: Molecular Regulation and Association with Neurological Disorders. *Neural Plast*. 2016:5136286

Hu J, Mukhopadhyay A, Craig AWB. 2011. Transducer of Cdc42-dependent Actin Assembly Promotes Epidermal Growth Factor-induced Cell Motility and Invasiveness*. *J Biol Chem*. 286(3):2261–72

Jacquemet G, Stubb A, Saup R, Miihkinen M, Kremneva E, et al. 2019. Filopodome Mapping Identifies p130Cas as a Mechanosensitive Regulator of Filopodia Stability. *Curr Biol*. 29(2):202-216.e7

Kadzik RS, Homa KE, Kovar DR. 2020. F-Actin Cytoskeleton Network Self-Organization Through Competition and Cooperation. *Annu Rev Cell Dev Bi*. 36(1):35–60

Kakimoto T, Katoh H, Negishi M. 2006. Regulation of Neuronal Morphology by Toca-1, an F-BAR/EFC Protein That Induces Plasma Membrane Invagination. *J Biol Chem*. 281(39):29042–53

Koestler SA, Steffen A, Nemethova M, Winterhoff M, Luo N, et al. 2013. Arp2/3 complex is essential for actin network treadmilling as well as for targeting of capping protein and cofilin. *Mol. Biol. Cell*. 24(18):2861–75

Koser DE, Thompson AJ, Foster SK, Dwivedy A, Pillai EK, et al. 2016. Mechanosensing is critical for axon growth in the developing brain. *Nat Neurosci*. 19(12):1592–98

Krause M, Leslie JD, Stewart M, Lafuente EM, Valderrama F, et al. 2004. Lamellipodin, an Ena/VASP Ligand, Is Implicated in the Regulation of Lamellipodial Dynamics. *Dev Cell*. 7(4):571–83

Laine RF, Tosheva KL, Gustafsson N, Gray RDM, Almada P, et al. 2019. NanoJ: a high-performance open-source super-resolution microscopy toolbox. *J. Phys. D: Appl. Phys.* 52(16):163001

Lebrand C, Dent EW, Strasser GA, Lanier LM, Krause M, et al. 2004. Critical Role of Ena/VASP Proteins for Filopodia Formation in Neurons and in Function Downstream of Netrin-1. *Neuron*. 42(1):37–49

Ledoux B, Zanin N, Yang J, Mercier V, Coster C, et al. 2023. Plasma membrane nanodeformations promote actin polymerization through CIP4/CDC42 recruitment and regulate type II IFN signaling. *Sci. Adv.* 9(50):eade1660

Lee K, Elliott HL, Oak Y, Zee C-T, Groisman A, et al. 2015. Functional Hierarchy of Redundant Actin Assembly Factors Revealed by Fine-Grained Registration of Intrinsic Image Fluctuations. *Cell Syst.* 1(1):37–50

Journal of Cell Science • Accepted manuscript

Lee K, Gallop JL, Rambani K, Kirschner MW. 2010. Self-Assembly of Filopodia-Like Structures on Supported Lipid Bilayers. *Science*. 329(5997):1341–45

Leung K-M, Holt CE. 2008. Live visualization of protein synthesis in axonal growth cones by microinjection of photoconvertible Kaede into Xenopus embryos. *Nat Protoc*. 3(8):1318–27

Li Y, Mund M, Hoess P, Deschamps J, Matti U, et al. 2018. Real-time 3D single-molecule localization using experimental point spread functions. *Nat Methods*. 15(5):367–69

Liu W, Du W, Shang X, Wang L, Evelyn C, et al. 2019. Rational identification of a Cdc42 inhibitor presents a new regimen for long-term hematopoietic stem cell mobilization. *Leukemia*. 33(3):749–61

Mallavarapu A, Mitchison T. 1999. Regulated Actin Cytoskeleton Assembly at Filopodium Tips Controls Their Extension and Retraction. *J Cell Biology*. 146(5):1097–1106

Mancinelli G, Lamparter L, Nosov G, Saha T, Pawluchin A, et al. 2021. Dendrite tapering actuates a self-organizing signaling circuit for stochastic filopodia initiation in neurons. *Proc National Acad Sci*. 118(43):e2106921118

Mattila PK, Pykäläinen A, Saarikangas J, Paavilainen VO, Vihinen H, et al. 2007. Missing-in-metastasis and IRSp53 deform PI(4,5)P2-rich membranes by an inverse BAR domain–like mechanism. *J Cell Biology*. 176(7):953–64

McCormick LE, Suarez C, Herring LE, Cannon KS, Kovar DR, et al. 2023. Multi-monoubiquitination controls VASP-mediated actin dynamics. *bioRxiv*. 2023.07.16.549237

McDonald NA, Vander Kooi CW, Ohi MD, Gould KL. 2015. Oligomerization but Not Membrane Bending Underlies the Function of Certain F-BAR Proteins in Cell Motility and Cytokinesis. *Dev Cell*. 35(6):725–36

Nakagawa H, Miki H, Nozumi M, Takenawa T, Miyamoto S, et al. 2003. IRSp53 is colocalised with WAVE2 at the tips of protruding lamellipodia and filopodia independently of Mena. *J. Cell Sci.* 116(12):2577–83

Noh J, Isogai T, Chi J, Bhatt K, Danuser G. 2022. Granger-causal inference of the lamellipodial actin regulator hierarchy by live cell imaging without perturbation. *Cell Syst*. 13(6):471-487.e8

Nozumi M, Nakatsu F, Katoh K, Igarashi M. 2017. Coordinated Movement of Vesicles and Actin Bundles during Nerve Growth Revealed by Superresolution Microscopy. *Cell Reports*. 18(9):2203–16

O'Connor T, Duerr J, Bentley D. 1990. Pioneer growth cone steering decisions mediated by single filopodial contacts in situ. *J Neurosci*. 10(12):3935–46

Journal of Cell Science • Accepted manuscript

Padrick SB, Rosen MK. 2010. Physical Mechanisms of Signal Integration by WASP Family Proteins. *Annu Rev Biochem*. 79(1):707–35

Peterson JR, Lebensohn AM, Pelish HE, Kirschner MW. 2006. Biochemical Suppression of Small-Molecule Inhibitors: A Strategy to Identify Inhibitor Targets and Signaling Pathway Components. *Chem. Biol.* 13(4):443–52

Pokrant T, Hein JI, Körber S, Disanza A, Pich A, et al. 2023. Ena/VASP clustering at microspike tips involves lamellipodin but not I-BAR proteins, and absolutely requires unconventional myosin-X. *Proc National Acad Sci*. 120(2):e2217437120

Pylvänäinen JW, Laine RF, Saraiva BMS, Ghimire S, Follain G, et al. 2023. Fast4DReg: Fast registration of 4D microscopy datasets. *J. Cell Sci.* 136(4):jcs260728

Qualmann B, Kelly RB. 2000. Syndapin Isoforms Participate in Receptor-Mediated Endocytosis and Actin Organization. *The Journal of Cell Biology*

Saengsawang W, Mitok K, Viesselmann C, Pietila L, Lumbard DC, et al. 2012. The F-BAR Protein CIP4 Inhibits Neurite Formation by Producing Lamellipodial Protrusions. *Curr Biol*. 22(6):494–501

Saengsawang W, Taylor KL, Lumbard DC, Mitok K, Price A, et al. 2013. CIP4 coordinates with phospholipids and actin-associated proteins to localize to the protruding edge and produce actin ribs and veils. *J Cell Sci*. 126(11):2411–23

Schindelin J, Arganda-Carreras I, Frise E, Kaynig V, Longair M, et al. 2012. Fiji: an open-source platform for biological-image analysis. . 9:676–82

Schwarz G. 1978. Estimating the Dimension of a Model. *Ann. Stat.* 6(2):

Shaner NC, Lambert GG, Chammas A, Ni Y, Cranfill PJ, et al. 2013. A bright monomeric green fluorescent protein derived from Branchiostoma lanceolatum. *Nat Methods*. 10(5):407–9

She B-R, Liou G-G, Lin-Chao S. 2002. Association of the Growth-Arrest-Specific Protein Gas7 with F-Actin Induces Reorganization of Microfilaments and Promotes Membrane Outgrowth. *Exp Cell Res*. 273(1):34–44

Shimada A, Takano K, Shirouzu M, Hanawa-Suetsugu K, Terada T, et al. 2010. Mapping of the basic amino-acid residues responsible for tubulation and cellular protrusion by the EFC/F-BAR domain of pacsin2/Syndapin II. *Febs Lett*. 584(6):1111–18

Skruber K, Warp PV, Shklyarov R, Thomas JD, Swanson MS, et al. 2020. Arp2/3 and Mena/VASP Require Profilin 1 for Actin Network Assembly at the Leading Edge. *Curr Biol*. 30(14):2651-2664.e5

Sudhaharan T, Hariharan S, Lim JSY, Liu JZ, Koon YL, et al. 2019. Superresolution microscopy reveals distinct localisation of full length IRSp53 and its I-BAR domain protein within filopodia. *Sci Rep-uk*. 9(1):2524

Journal of Cell Science • Accepted manuscript

Taylor KL, Taylor RJ, Richters KE, Huynh B, Carrington J, et al. 2019. Opposing functions of F-BAR proteins in neuronal membrane protrusion, tubule formation, and neurite outgrowth. *Life Sci Alliance*. 2(3):e201800288

Tinevez J-Y, Perry N, Schindelin J, Hoopes GM, Reynolds GD, et al. 2017. TrackMate: An open and extensible platform for single-particle tracking. *Methods*. 115:80–90

Truesdell P, Ahn J, Chander H, Meens J, Watt K, et al. 2015. CIP4 promotes lung adenocarcinoma metastasis and is associated with poor prognosis. *Oncogene*. 34(27):3527–35

Tsai F-C, Bertin A, Bousquet H, Manzi J, Senju Y, et al. 2018. Ezrin enrichment on curved membranes requires a specific conformation or interaction with a curvature-sensitive partner. *Elife*. 7:e37262

Tsai F-C, Henderson JM, Jarin Z, Kremneva E, Senju Y, et al. 2022. Activated I-BAR IRSp53 clustering controls the formation of VASP-actin–based membrane protrusions. *Sci Adv*. 8(41):eabp8677

Tsujita K, Suetsugu S, Sasaki N, Furutani M, Oikawa T, Takenawa T. 2006. Coordination between the actin cytoskeleton and membrane deformation by a novel membrane tubulation domain of PCH proteins is involved in endocytosis. *J Cell Biology*. 172(2):269–79

Urbančič V, Butler R, Richier B, Peter M, Mason J, et al. 2017. Filopodyan: An open-source pipeline for the analysis of filopodia. *J Cell Biology*. 216(10):3405–22

Walrant A, Saxton DS, Correia GP, Gallop JL. 2015. Chapter 8 Triggering actin polymerization in Xenopus egg extracts from phosphoinositide-containing lipid bilayers. *Methods Cell Biol*. 128:125–47

Wang Y, Schnitzbauer J, Hu Z, Li X, Cheng Y, et al. 2014. Localization events-based sample drift correction for localization microscopy with redundant cross-correlation algorithm. *Opt Express*. 22(13):15982

Welf ES, Danuser G. 2014. Using Fluctuation Analysis to Establish Causal Relations between Cellular Events without Experimental Perturbation. *Biophys J*. 107(11):2492–98

Wit CB, Hiesinger PR. 2022. Neuronal filopodia: From stochastic dynamics to robustness of brain morphogenesis. *Semin Cell Dev Biol*. 133:10–19

Zhai X, Shen Y, Zhang X, Li T, Lu Q, Xu Z. 2022. FCHSD2 cooperates with CDC42 and N-WASP to regulate cell protrusion formation. *Biochimica Et Biophysica Acta Bba - Mol Cell Res*. 1869(1):119134

Zhang M, Chang H, Zhang Y, Yu J, Wu L, et al. 2012. Rational design of true monomeric and bright photoactivatable fluorescent proteins. *Nat Methods*. 9(7):727–29

Journal of Cell Science • Accepted manuscript

Figures

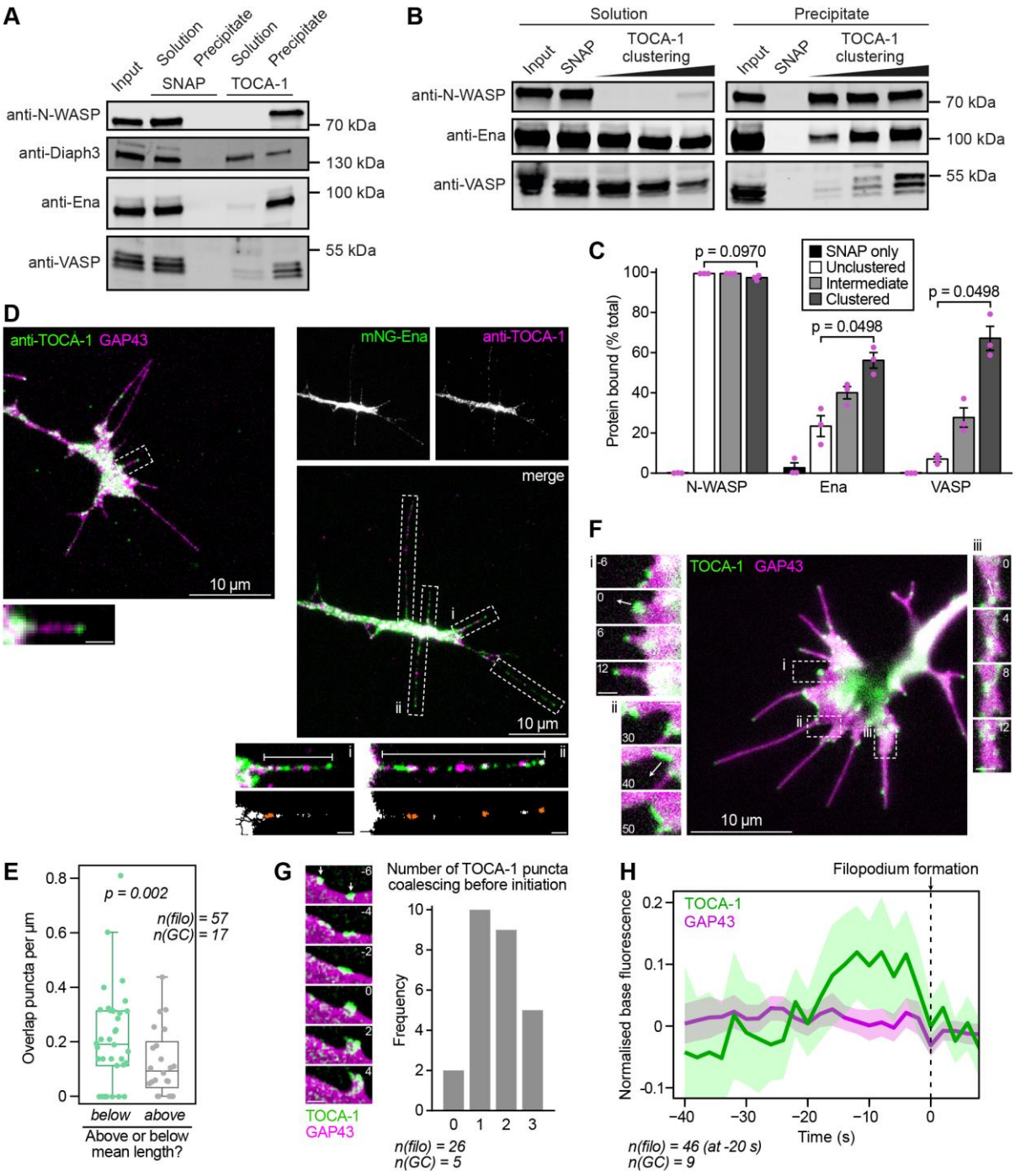

Fig. 1. TOCA-1 interacts with Ena and VASP and localises to filopodia

(A) SNAP alone or SNAP-TOCA-1 coupled to beads and incubated with *Xenopus* egg high speed supernatant extract (HSS), with Western blotting for known and candidate TOCA-1-interacting proteins. None of the proteins bound to SNAP alone, while all were bound by SNAP-TOCA-1. (B) 1 nmol SNAP-TOCA-1 was coupled to 10, 50 or 100 µl beads followed by

Journal of Cell Science • Accepted manuscript

addition of beads up to a volume of 100 µl and an excess of SNAP protein in a second coupling step. After incubation with HSS (containing ~90 pmol Ena, 30 pmol each VASP and N-WASP), Ena and VASP are bound more efficiently at higher densities of TOCA-1 while N-WASP binding efficiency is unaffected. Blots are representative of three repeats. (C) Quantification of protein bound in (B) (as percentage of precipitate + solution bands, bars show s.e.m). (D) Fixed RGCs expressing GAP43-RFP, immunostained with affinity purified anti-TOCA-1, showing puncta of TOCA-1 in shafts at tips (see example inset). Filopodia in fixed RGCs expressing mNG-Ena and immunostained against TOCA-1 show that both form multiple, distinct puncta along filopodia, sometimes at bases (i) and shafts, and sometimes at tips (ii), with manual quantification (white dashed boxes, with examples (i) and (ii) showing areas of TOCA-1/Ena overlap after thresholding, in orange) showing the number of overlapping puncta is around 30% of either Ena or TOCA-1 puncta numbers. (E) Grouping filopodia by size reveals that shorter filopodia have a higher density of TOCA-1 and Ena overlap puncta ($p = 0.002$; Kruskal-Wallis test). (F) A *Xenopus* RGC axonal growth cone (Movie 1) after electroporation with mNG-TOCA-1 and the membrane binding region of GAP43-RFP, showing localisation of mNG-TOCA-1 to (i) filopodia, (ii) advancing lamellipodia and (iii) inwardly-moving puncta in the growth cone body. Arrows show direction of punctum movement. (G) Example montage (Movie 2) shown with two distinct puncta indicated by arrows. Images de-noised with nd-safir. Scoring of the number of distinct puncta of mNG-TOCA-1 observed to coalesce in the preceding few seconds at the site of future filopodium formation. (H) Measuring fluorescence intensity of mNG-TOCA-1 and GAP43-RFP at the predicted base before formation, shows that mNG-TOCA-1 fluorescence peaks around 10 s prior to filopodium emergence and reduces before protrusion begins. Shading represents 95% confidence interval. All scale bars are 1 µm unless indicated, time shown in seconds.

Journal of Cell Science • Accepted manuscript

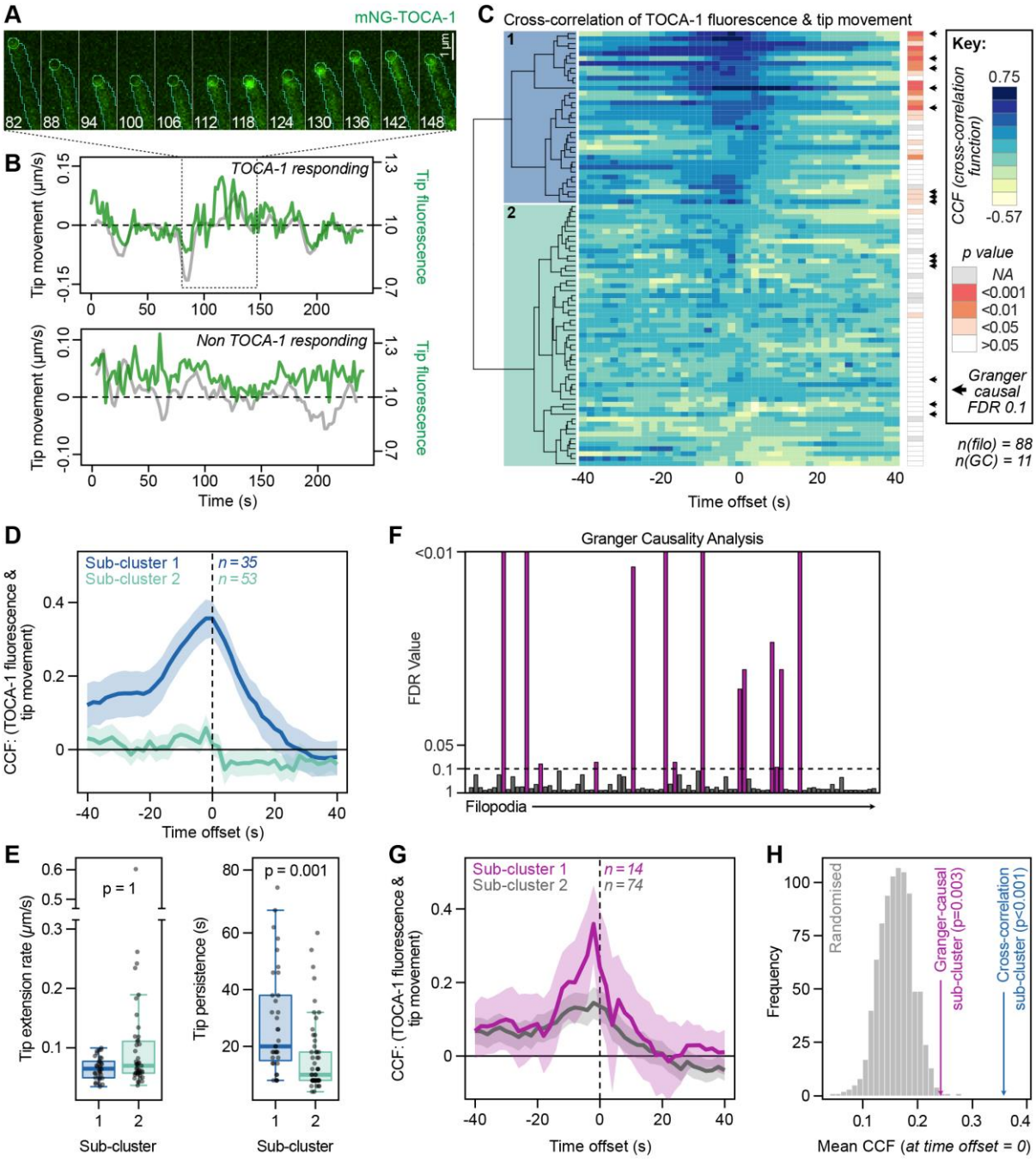

Fig. 2. TOCA-1 has a functional role during filopodial tip extension

(A) Montage of filopodia (cyan outline) and tip (green circle) segmented by Filopodyan, showing an increase in mNG-TOCA-1 fluorescence at the moment of forward movement. (B) Quantification of fluorescence intensity of two independent filopodia with distinct behaviours. (C) Cross-correlation functions (CCFs) for each filopodium at multiple time offsets between tip movement and tip TOCA-1 fluorescence, with hierarchical clustering based on CCFs from -6 to +6 s. Colour shows degree of correlation. Likelihood of the

Journal of Cell Science • Accepted manuscript

observed level of correlation occurring by chance in individual filopodia indicated by grey/orange boxes to the right, as computed using Markov Chain simulations. P values shown in the figure are not corrected for multiple comparisons. (D) Averaging the top-correlating, “TOCA-1-responding” sub-cluster (1 in (C), blue) separately from the rest of the filopodia (2 in (C), green) reveals a strong correlation between tip movement and fluorescence, peaking at -2 s time offset. Shading represents 95% confidence interval. (E) TOCA-1 responding filopodia (sub-cluster 1) have no change in tip extension rate, while persistence of tip movement (based on the auto-correlation function) is increased two-fold. (F) Granger causality analysis confirms that some of the TOCA-1 responding filopodia are Granger-causal for tip movement (black arrows in (C)), and (G) a TOCA-1 responding sub-cluster defined using this criterion still has greater mean cross-correlation. (H) A randomisation approach to testing significance shows that the observed degree of correlation in the TOCA-1 responding sub-cluster defined by cross-correlation (blue arrow) or GCA (purple arrow) is stronger than would be expected if TOCA-1 tip fluorescence and tip movement were decoupled, since out of 1000 reshuffled datasets, 0 and 3 respectively produced a sub-cluster with higher mean CCF at t=0.

Journal of Cell Science • Accepted manuscript

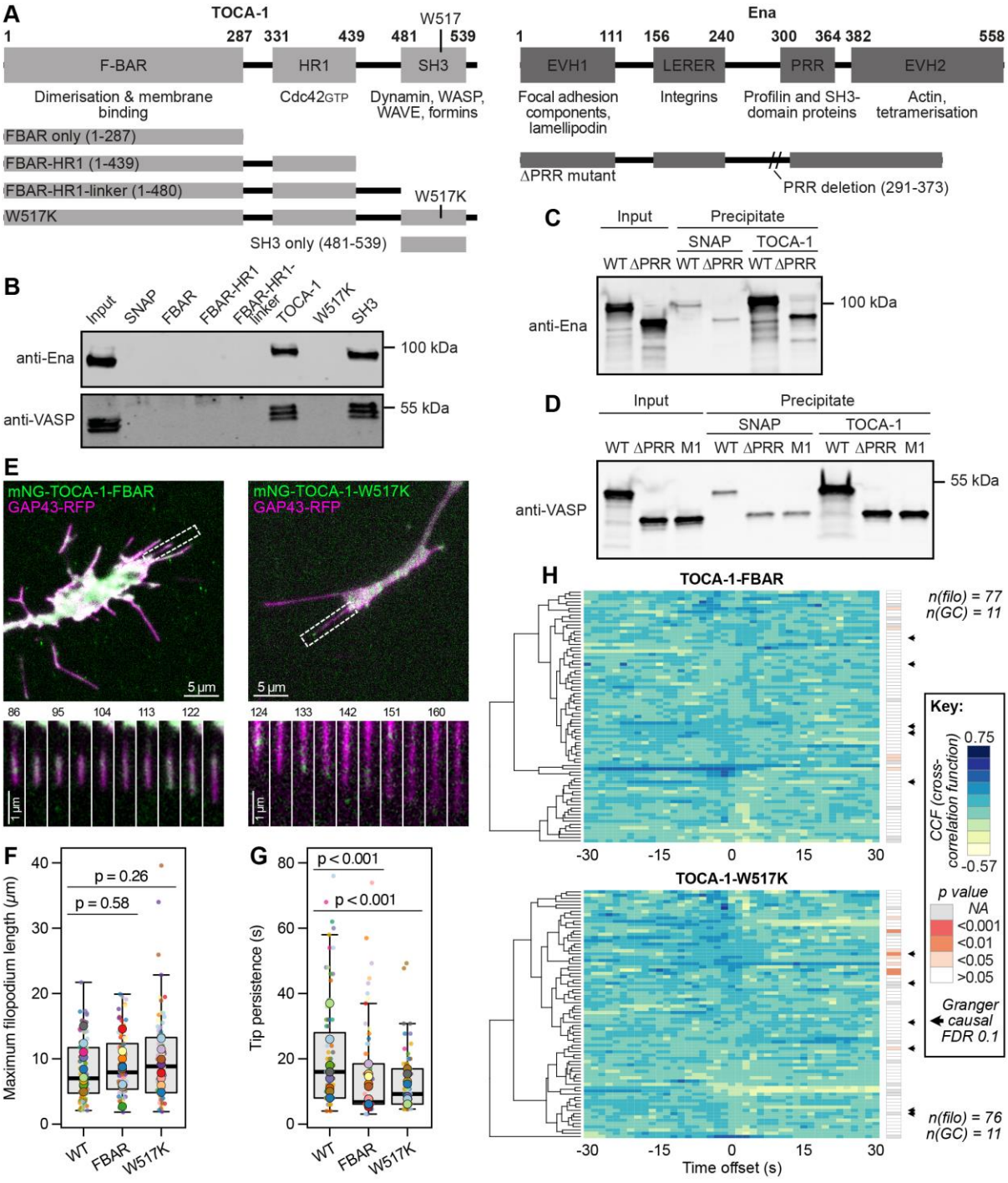

Fig. 3. An intact TOCA-1-SH3 domain is necessary for TOCA-1 function in filopodia

(A) Schematic of TOCA-1 and Ena domain structures and mutations used in this study, numbered according to *Xenopus* sequences. (B) The intact TOCA-1 SH3 domain is necessary and sufficient to bind Ena and VASP in HSS. (C) Purified TOCA-1 and Ena interact directly via the PRR of Ena. (D) Purified VASP and TOCA-1 interaction is not abolished by removal of the PRR or additional proline removal (M1 = ΔPRR + mutation of additional proline). (E)

Journal of Cell Science • Accepted manuscript

Truncation to the FBAR domain only and a W517K mutation (Movie 3) in the SH3 domain leads to fewer and more diffuse puncta. Time indicated in seconds. (F) The maximum length reached by filopodia on average was unchanged between wild type and mutant growth cones, and (G) the median tip persistence was reduced after expression of either TOCA-1 mutant. Significance assessed with Mann-Whitney tests, with multiple comparisons corrected using the Holm method. (H) Repeating the cross-correlation analysis for TOCA-1 mutants shows a greatly reduced correlation between tip fluorescence and tip movement in either mutant. Black arrows indicate filopodia where TOCA-1-FBAR/W517K fluorescence was Granger-causal for tip movement, which could be due to heterodimerisation with endogenous TOCA-1. P value assessed by Markov chain simulation.

Journal of Cell Science • Accepted manuscript

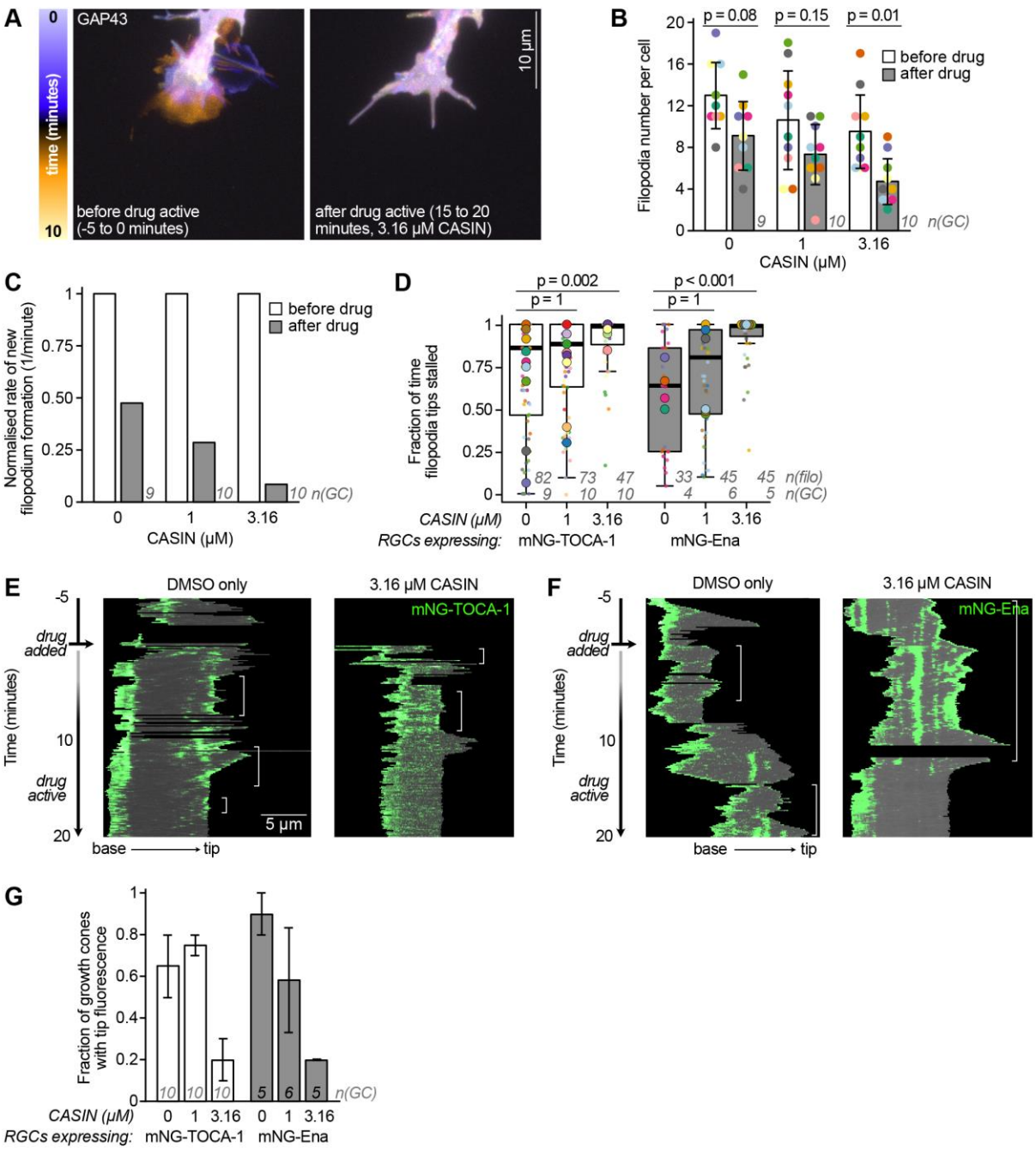

Fig. 4. Inhibition of Cdc42 with CASIN implicates TOCA-1 and Ena in Cdc42-driven filopodial protrusion

(A) A temporal projection of a RGC expressing GAP43-RFP and mNG-TOCA-1 imaged every 7.5 s before or after treatment with Cdc42 inhibitor CASIN (3.16 µM) showing the loss of growth cone activity, see Movie 4. (B) The number of filopodia per growth cone before and after drug treatment, showing a moderate decrease at higher CASIN concentration. Circles show the mean for each growth cone, error bars show standard deviation. (C) The rate of new filopodia formation per minute before and after drug treatment, showing a large

Journal of Cell Science • Accepted manuscript

decrease in filopodial initiation with CASIN treatment. Values normalised to the rate before treatment, excluding filopodia that were longer than 2 µm in their first frame. Data in (B) and (C) for RGCs expressing mNG-TOCA-1; results for mNG-Ena were similar. (D) CASIN causes stalling of filopodia tips in RGCs expressing either mNG-TOCA-1 or mNG-Ena. Circles show the median for each growth cone, with matched coloured dots for each filopodium. (E) Representative example of filopodium growth and retraction with mNG-TOCA-1 fluorescence over the timecourse of CASIN or DMSO addition shown in a kymograph with filopodium base on the left and tip on the right. Time periods with tip fluorescence are indicated with a white bracket. With CASIN, TOCA-1 fluorescence disappears, one round of protrusion continues and then both TOCA-1 localisation and filopodial protrusion cease. (F) Individual representative example of mNG-Ena fluorescence similarly disappearing during the last round of filopodial protrusion similar to (E). (G) The fraction of growth cones after drug treatment that still had any filopodia tip fluorescence decreased for RGCs expressing mNG-TOCA-1 and mNG-Ena, in a dose-responsive manner. Mean of two independent assessments, error bars show range. N numbers are indicated on the plots. Significance assessed with Mann-Whitney tests, with multiple comparisons corrected using the Holm method.

Journal of Cell Science • Accepted manuscript

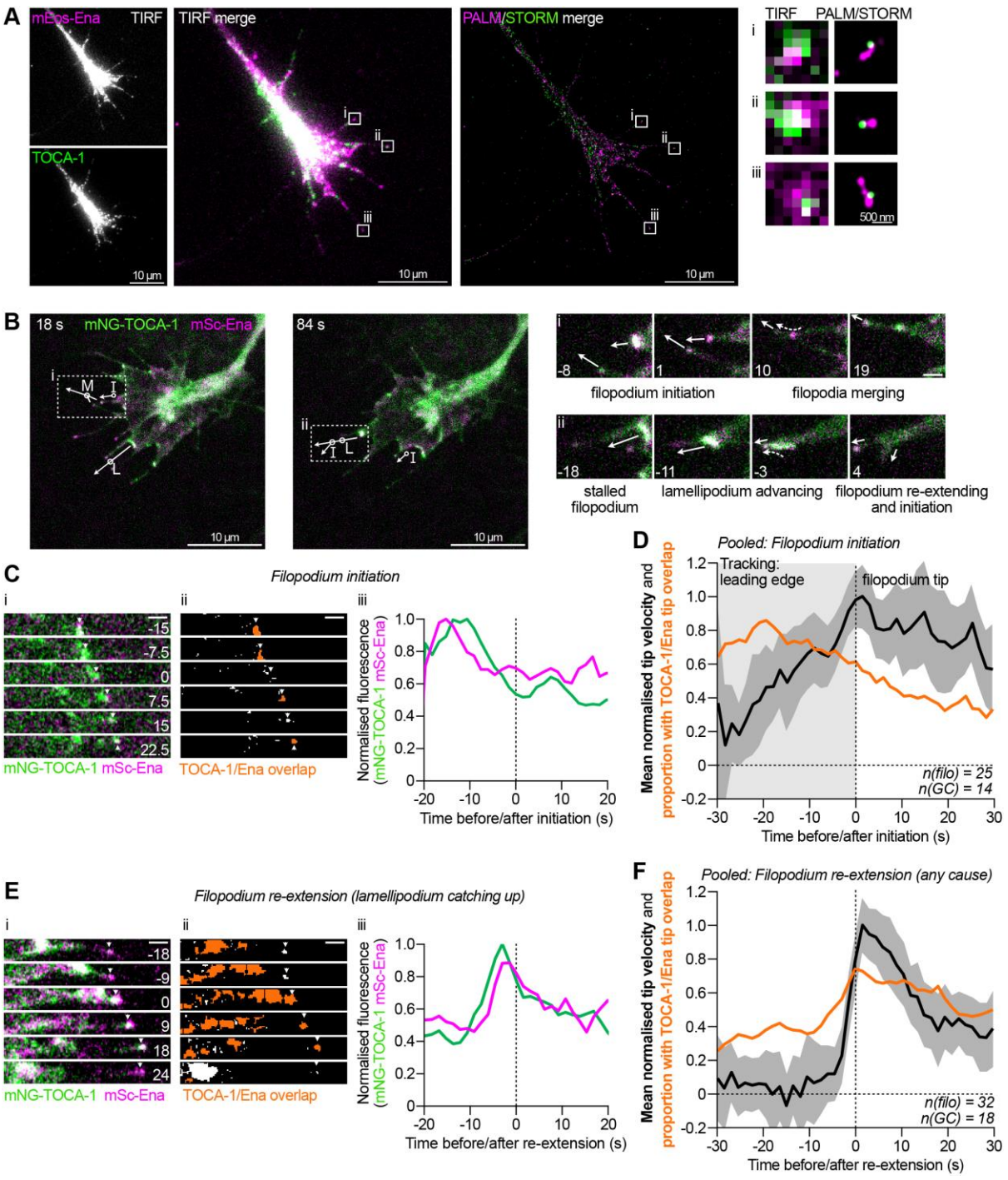

Fig. 5. TOCA-1 and Ena coincide transiently during filopodial initiation and re-extension

(A) 2-colour PALM/STORM imaging of fixed RGCs expressing mEos-Ena and immunostained against TOCA-1 (TIRF reference images, *left*). This confirms that many filopodia have both Ena and TOCA-1 at tips (features i-iii), however, there is no consistent arrangement of the two proteins, indicating there is no stable, structured complex. (B) 57 filopodial protrusion events were collected from 2-colour, simultaneous TIRF imaging of RGCs injected with mNG-

Journal of Cell Science • Accepted manuscript

TOCA-1 and mScarlet-Ena; 3 minutes at 1.5 s per frame) and assigned as initiation (25/57) or re-extension (32/57). In these examples (both from Movie 5) multiple protrusion events were observed and some filopodia were observed undergoing two types of events. Arrows indicate ongoing/future tip movement for selected protruding filopodia, with circles showing site of protrusion event (I = initiation, L = re-extension after lamellipodium catching up, M = re-extension after merging of a second filopodium). Boxes i and ii are shown expanded (*right*) to show time course of compound protrusion events. Arrows indicate ongoing/future tip movement, dashed arrows indicate movement of fluorescent TOCA-1/Ena puncta towards tips. (C) Montages showing (i) the advancing tip position (arrows in C, E), (ii) the presence of TOCA-1/Ena overlap (orange regions in C, E) and (iii) the fluorescence intensity of TOCA-1 and Ena before and after initiation. (D) Pooling 25 initiation events confirms that the prevalence of TOCA-1/Ena overlap at tips (orange line) was high before initiation before gradually falling to low levels, while the mean velocity of the tip peaked around initiation (black line, shading represents 95% confidence interval). (E) Montages showing re-extension events caused by the lamellipodium catching up with a static filopodium, with (i) the advancing tip position, (ii) areas of TOCA-1/Ena overlap, including large areas of the lamellipodium and (iii) the fluorescence intensity of TOCA-1 and Ena at the tip shows a peak shortly before re-extension. (F) Pooling 32 re-extension events confirms that TOCA-1/Ena overlap levels (orange line) at static tips are low, rising to high levels around re-extension, as seen by the transient burst of high mean tip velocity (black line, shading represents 95% confidence interval). All scale bars 1 µm unless indicated, time indicated in seconds relative to initiation/re-extension event.

Journal of Cell Science • Accepted manuscript

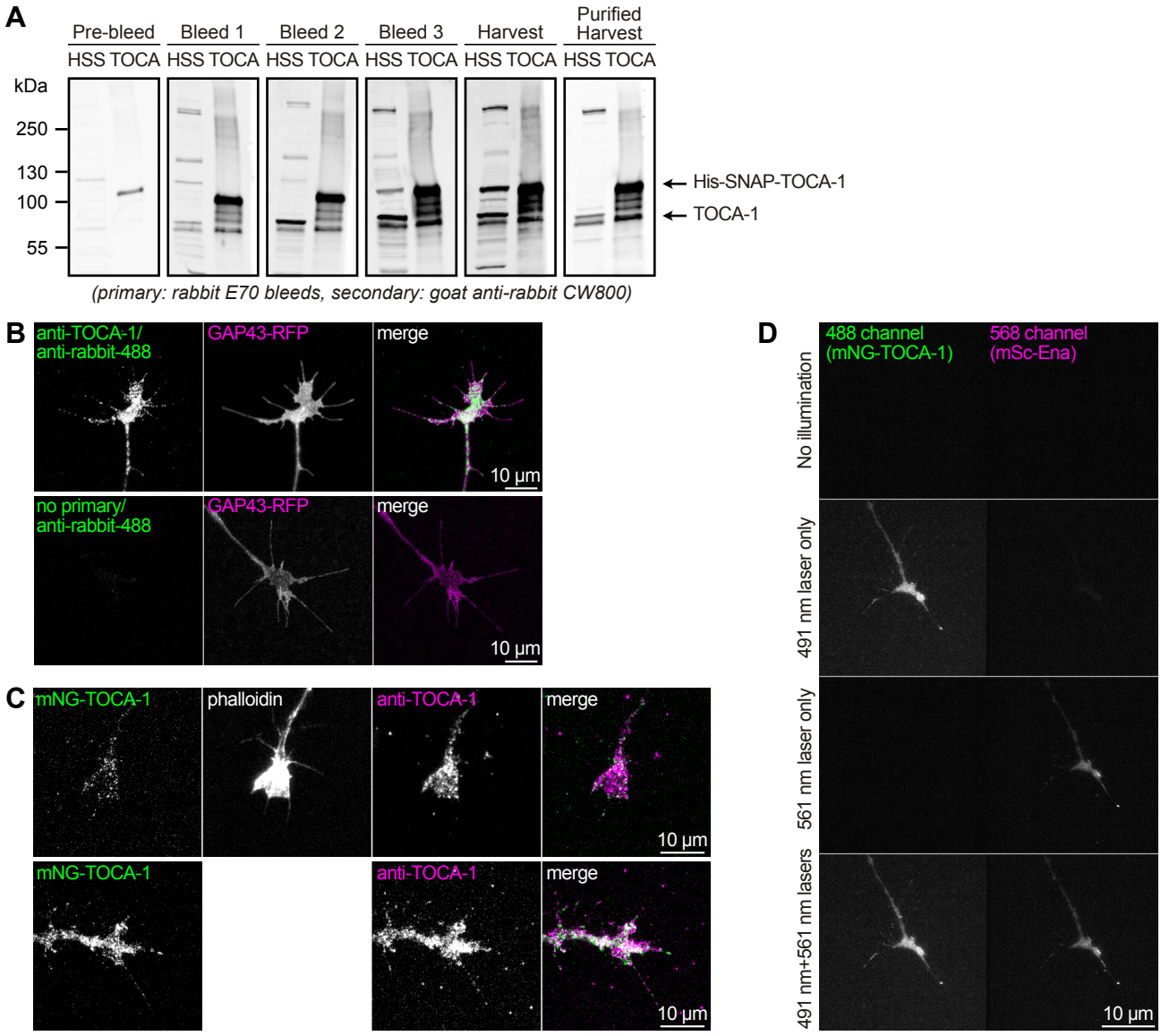

Fig. S1. Affinity purified rabbit anti-TOCA-1 antibody recognises TOCA-1 in lysate and cells.

(A) SDS-PAGE gel with *Xenopus* egg extract (HSS) or purified SNAP-TOCA-1 (TOCA), stained with the indicated bleeds at 1:500 dilution, showing that before immunisation, a small non-specific band was present with concentrated, purified SNAP-TOCA-1 and not with HSS. All post-immunisation bleeds recognise TOCA-1 in HSS and purified SNAP-TOCA-1, and after affinity purification ("purified harvest") the specificity is greatly improved. (B) RGCs expressing membrane marker GAP43-RFP. No primary antibody immunostaining control, showing that fluorescence is specific to anti-TOCA-1/anti-rabbit-488. Contrast applied equally between images for 488 channel and allowed to vary in GAP43-RFP channel to account for variable expression levels. (C) RGCs expressing mNG-TOCA-1, immunostained with anti-TOCA-1 / anti-rabbit-AF647 and phalloidin-AF568, showing a similar pattern of fluorescence between endogenous and exogenous TOCA-1. (D) Acquiring images with no, one or both lasers active confirmed that almost no fluorescent signal in the 568 channel was due to excitation of either fluorophore with the 491 nm laser, and vice versa. No background subtraction, contrast applied equally to all eight images.

Journal of Cell Science • Supplementary information

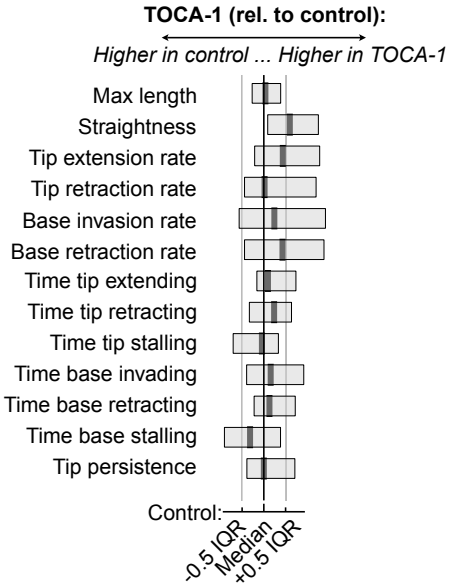

Fig. S2. Overexpression of mNG-TOCA-1 does not affect filopodial dynamics
Filopodia from RGCs electroporated with mRNA for membrane marker GAP43-RFP and either mNG-TOCA-1 or mNG alone were analysed with Filopodyan, revealing no significant differences in filopodia parameters. Boxes show median and IQR of mNG-TOCA-1 data, grid lines show median and IQR for control data; see Table S1 for full data.

Journal of Cell Science • Supplementary information

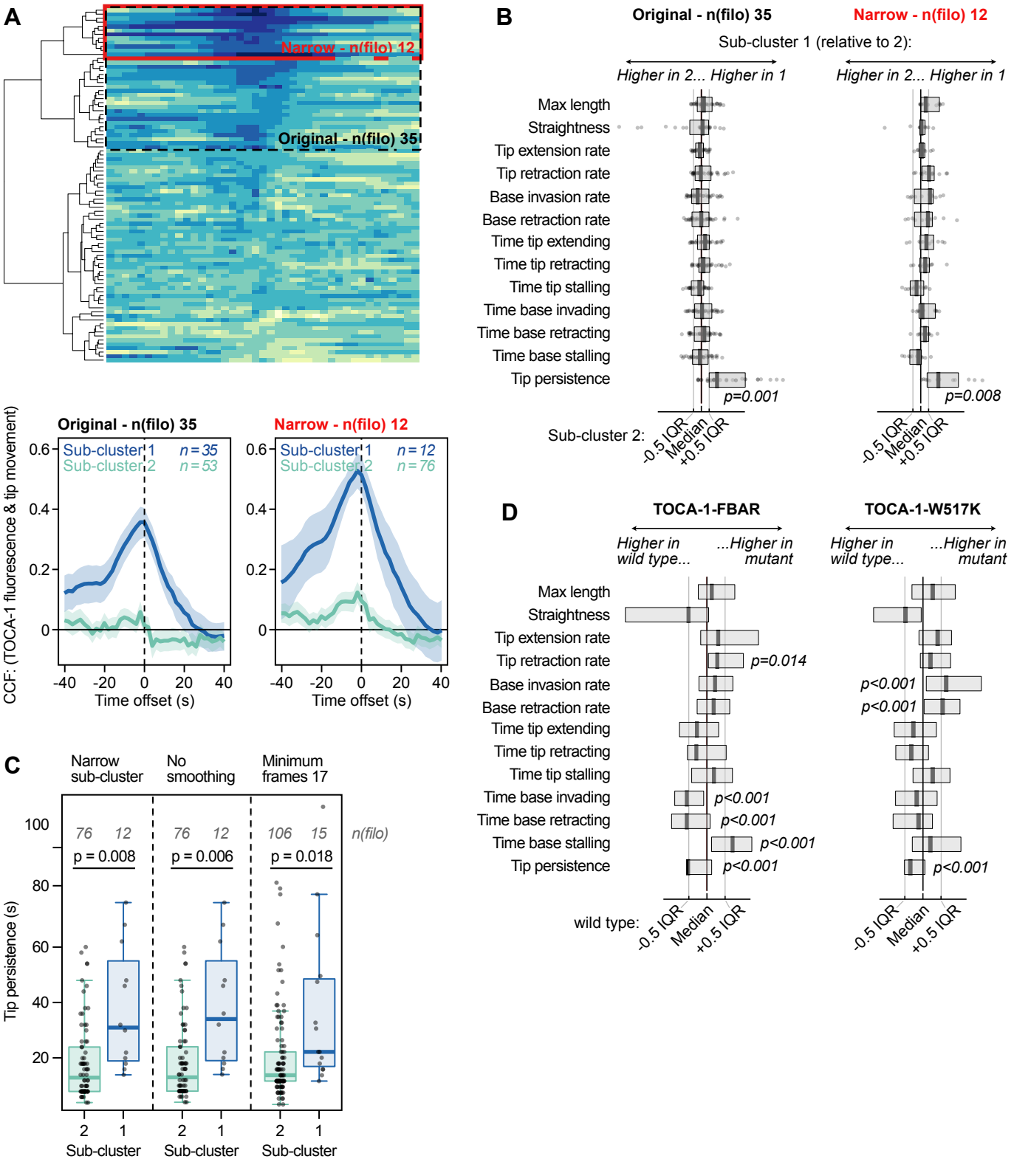

Journal of Cell Science • Supplementary information

Fig. S3. TOCA-1 tip fluorescence correlates with tip movement, producing a high tip persistence sub-cluster, across varying processing parameters

(A) Varying the sub-cluster point after hierarchical clustering (heatmap adapted from Fig. 2C) still produces a TOCA-1 responding sub-cluster (high mean cross-correlation score peaking with a lag of -2 s). "Original" line graph adapted from Fig. 2D. (B) Both the original and narrow sub-clusters have significantly higher median tip persistence, but no other significant morphological changes. (C) Varying data processing parameters such as altering the sub-clustering point (see (A)), removing smoothing of tip movement data or reducing the minimum frames threshold for inclusion of a filopodium still produces a TOCA-1 responding sub-cluster with significantly higher tip persistence than non responding filopodia. (D) Both TOCA-1 mutants led to significantly reduced tip persistence, with other significant changes including in filopodial base dynamics. Significance tested by Mann-Whitney test after Holm correction for multiple comparisons and shown where $p < 0.05$, n(filo) shown on graphs; all data n(GC) = 11.

Journal of Cell Science • Supplementary information

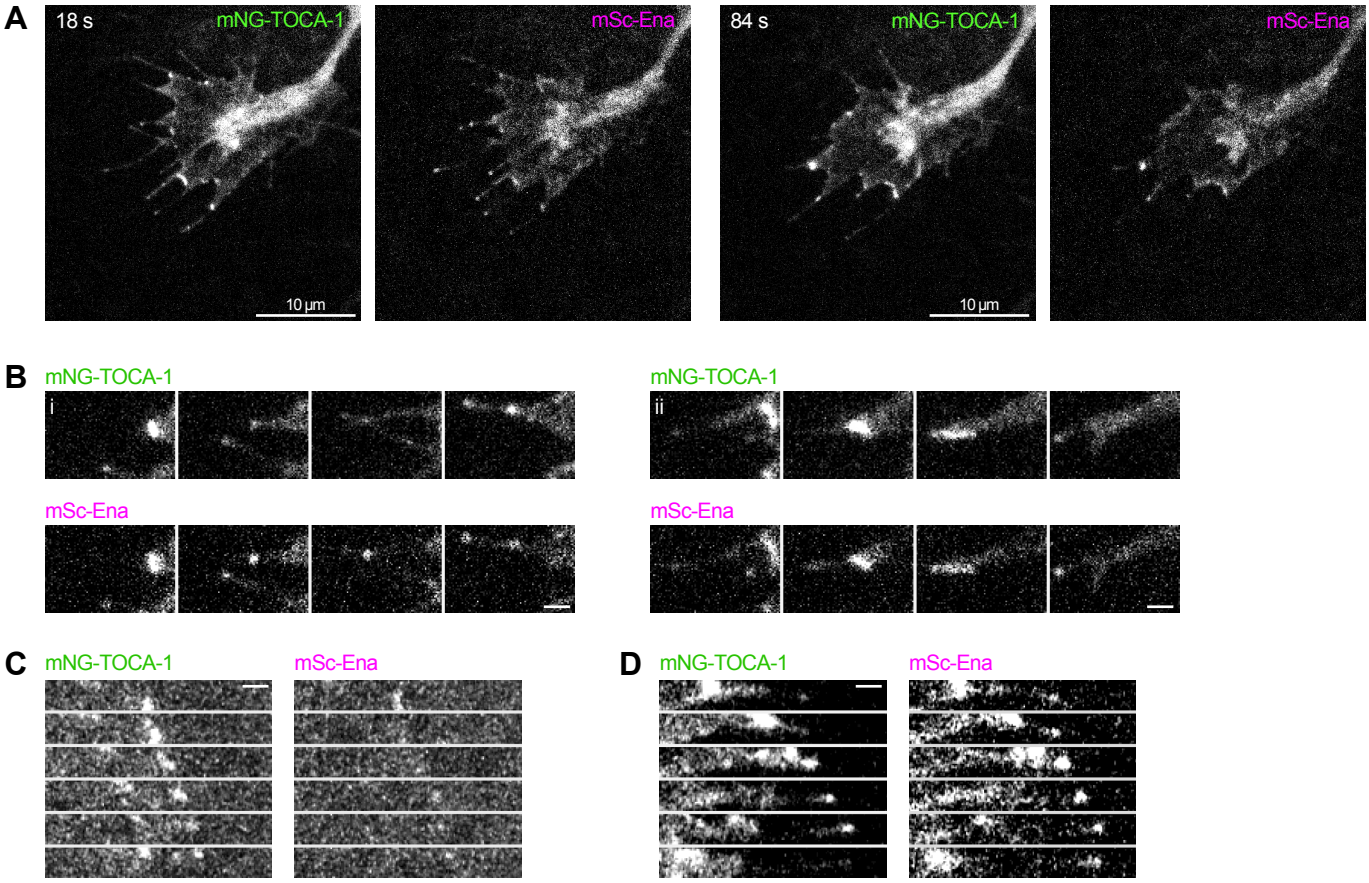

Fig. S4. Single channel images of RGCs expressing mNG-TOCA-1 and mSc-Ena
Images of mNG-TOCA-1 and mSc-Ena relating to (A) Fig. 5B, (B) Fig. 5Bi and Bii, (C) Fig. 5Ci, and (D) Fig. 5Ei. Scale bars 1 µm unless stated.

Journal of Cell Science • Supplementary information

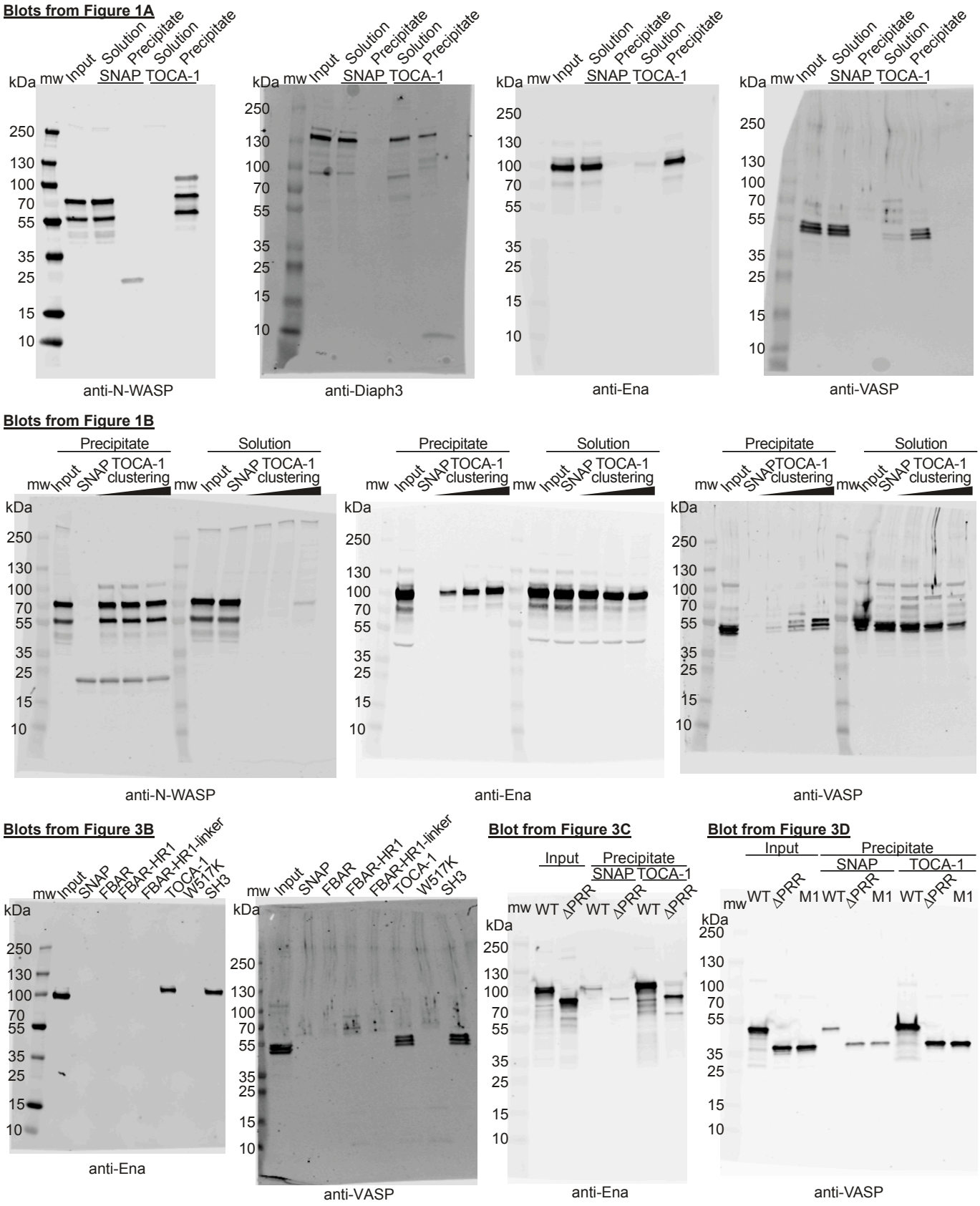

Fig. S5. Uncropped Western blots relating to Fig. 1 and Fig. 3

Journal of Cell Science • Supplementary information

Table S1. Filopodia dynamics parameters from Filopodyan, showing no difference between mNG alone and mNG-TOCA-1.

TOCA-1 vs CTRL (Fig S2)

Parameter	*Condition*	*Min.*	*1st Qu.*	*Median*	*Mean*	*3rd Qu.*	*Max.*	*SD*	*N*
Max length	CTRL	2.000	2.718	4.993	6.783	11.212	17.039	4.74	63
Max length	TOCA-1	1.852	2.798	5.292	6.536	8.162	21.708	4.63	80
Straightness	CTRL	0.652	0.882	0.897	0.883	0.918	0.935	0.06	31
Straightness	TOCA-1	0.607	0.900	0.918	0.892	0.941	0.980	0.09	41
Tip extension rate	CTRL	0.038	0.045	0.053	0.061	0.070	0.124	0.02	41
Tip extension rate	TOCA-1	0.035	0.048	0.064	0.073	0.084	0.181	0.03	62
Tip retraction rate	CTRL	0.033	0.051	0.055	0.060	0.070	0.112	0.02	35
Tip retraction rate	TOCA-1	0.035	0.047	0.055	0.070	0.078	0.198	0.04	50
Base invasion rate	CTRL	0.034	0.047	0.053	0.060	0.063	0.128	0.02	43
Base invasion rate	TOCA-1	0.035	0.045	0.057	0.061	0.075	0.128	0.02	66
Base retraction rate	CTRL	0.035	0.045	0.055	0.056	0.062	0.101	0.02	46
Base retraction rate	TOCA-1	0.035	0.048	0.062	0.065	0.078	0.143	0.02	65
Time tip extending	CTRL	0.000	0.004	0.182	0.255	0.457	0.800	0.24	55
Time tip extending	TOCA-1	0.000	0.112	0.223	0.321	0.504	1.000	0.28	72
Time tip retracting	CTRL	0.000	0.000	0.052	0.113	0.162	1.000	0.17	55
Time tip retracting	TOCA-1	0.000	0.000	0.089	0.110	0.151	1.000	0.15	72
Time tip stalling	CTRL	0.000	0.412	0.649	0.632	0.879	1.000	0.29	55
Time tip stalling	TOCA-1	0.000	0.332	0.629	0.569	0.800	1.000	0.29	72
Time base invading	CTRL	0.000	0.017	0.121	0.133	0.198	0.667	0.13	57
Time base invading	TOCA-1	0.000	0.052	0.148	0.188	0.281	1.000	0.19	73
Time base retracting	CTRL	0.000	0.029	0.162	0.214	0.250	1.000	0.26	57
Time base retracting	TOCA-1	0.000	0.115	0.190	0.227	0.316	1.000	0.19	73
Time base stalling	CTRL	0.000	0.525	0.681	0.653	0.851	1.000	0.27	57
Time base stalling	TOCA-1	0.000	0.397	0.582	0.585	0.802	1.000	0.25	73
Tip persistence	CTRL	4.000	10.000	16.000	19.321	26.000	60.000	12.25	53
Tip persistence	TOCA-1	4.000	10.000	16.000	22.306	27.000	106.00	19.49	72

TOCA-1 vs CTRL (Fig S2)

	Fold change (median)	*Fold change (mean)*	*z-score*	*Cliff's delta*	*P (Mann-Whitney)*	*P (Holm-adjusted)*
Max length	1.0599	0.9636	-0.0520	-0.0222	0.8215	1.0000
Straightness	1.0234	1.0106	0.1520	0.3375	0.0143	0.1858
Tip extension rate	1.1987	1.2010	0.5745	0.1853	0.1134	0.9069
Tip retraction rate	1.0059	1.1552	0.4851	0.0629	0.6265	1.0000
Base invasion rate	1.0693	1.0189	0.0515	0.0254	0.8258	1.0000
Base retraction rate	1.1299	1.1499	0.5362	0.2475	0.0270	0.3237
Time tip extending	1.2275	1.2581	0.2691	0.1424	0.1693	1.0000
Time tip retracting	1.7121	0.9727	-0.0179	0.0523	0.6097	1.0000
Time tip stalling	0.9692	0.9006	-0.2187	-0.1258	0.2263	1.0000
Time base invading	1.2275	1.4077	0.4100	0.1901	0.0633	0.6960
Time base retracting	1.1695	1.0617	0.0515	0.1702	0.0967	0.9065
Time base stalling	0.8542	0.8965	-0.2544	-0.1735	0.0907	0.9065
Tip persistence	1.0000	1.1545	0.2436	0.0128	0.9042	1.0000

Table S2. Filopodia dynamics parameters from Filopodyan, showing that TOCA-1 responding filopodia had significantly increased tip persistence compared to others.

Sub-cluster 1 vs Sub-cluster 2 (Fig. 3C)

Parameter	*Sub-cluster*	*Min.*	*1st Qu.*	*Median*	*Mean*	*3rd Qu.*	*Max.*	*SD*	*N*
Max length	2	2.119	4.213	6.933	8.170	11.518	21.708	4.82	53
Max length	1	2.077	5.041	8.115	8.698	11.938	17.232	4.35	35
Straightness	2	0.453	0.879	0.917	0.857	0.923	0.973	0.14	36
Straightness	1	0.687	0.885	0.920	0.896	0.937	0.980	0.07	26
Tip extension rate	2	0.036	0.057	0.070	0.101	0.111	0.602	0.09	45
Tip extension rate	1	0.034	0.050	0.064	0.065	0.077	0.100	0.02	34
Tip retraction rate	2	0.038	0.047	0.066	0.084	0.088	0.257	0.06	43
Tip retraction rate	1	0.039	0.050	0.065	0.075	0.092	0.150	0.03	35
Base invasion rate	2	0.034	0.054	0.070	0.074	0.087	0.178	0.03	51
Base invasion rate	1	0.039	0.050	0.062	0.068	0.086	0.113	0.02	35
Base retraction rate	2	0.036	0.057	0.066	0.069	0.078	0.134	0.02	51
Base retraction rate	1	0.042	0.053	0.066	0.067	0.077	0.116	0.02	35
Time tip extending	2	0.000	0.085	0.211	0.241	0.371	0.744	0.20	53
Time tip extending	1	0.000	0.140	0.280	0.269	0.356	0.603	0.17	35
Time tip retracting	2	0.000	0.017	0.127	0.130	0.191	0.435	0.12	53
Time tip retracting	1	0.021	0.100	0.151	0.172	0.220	0.443	0.11	35
Time tip stalling	2	0.148	0.380	0.661	0.629	0.856	1.000	0.26	53
Time tip stalling	1	0.102	0.356	0.600	0.559	0.733	0.969	0.23	35
Time base invading	2	0.000	0.153	0.205	0.213	0.297	0.463	0.11	53
Time base invading	1	0.059	0.143	0.212	0.221	0.302	0.400	0.10	35
Time base retracting	2	0.000	0.167	0.263	0.249	0.345	0.473	0.12	53
Time base retracting	1	0.042	0.183	0.297	0.281	0.356	0.482	0.12	35
Time base stalling	2	0.159	0.390	0.517	0.538	0.667	1.000	0.21	53
Time base stalling	1	0.164	0.361	0.492	0.498	0.637	0.885	0.19	35
Tip persistence	2	4.000	8.000	10.000	16.038	18.000	60.000	12.89	53
Tip persistence	1	8.000	15.000	20.000	28.400	38.000	76.00	18.61	35

Sub-cluster 1 vs Sub-cluster 2 (Fig. 3C)

	Fold change (median)	*Fold change (mean)*	*Cliff's delta*	*P (Mann-Whitney)*	*P (Holm-adjusted)*
Max length	1.1705	1.0646	0.1008	0.4278	1.0000
Straightness	1.0039	1.0459	0.1325	0.3830	1.0000
Tip extension rate	0.9275	0.6456	-0.2170	0.1013	1.0000
Tip retraction rate	0.9798	0.8985	0.0545	0.6841	1.0000
Base invasion rate	0.8914	0.9270	-0.1126	0.3794	1.0000
Base retraction rate	0.9987	0.9650	-0.0370	0.7751	1.0000
Time tip extending	1.3284	1.1151	0.1429	0.2602	1.0000
Time tip retracting	1.1854	1.3212	0.2345	0.0641	0.7695
Time tip stalling	0.9077	0.8894	-0.1682	0.1849	1.0000
Time base invading	1.0317	1.0368	0.0237	0.8546	1.0000
Time base retracting	1.1290	1.1294	0.1369	0.2808	1.0000
Time base stalling	0.9508	0.9256	-0.0895	0.4818	1.0000
Tip persistence	2.0000	1.7708	0.4868	0.0001	0.0014

Journal of Cell Science • Supplementary information

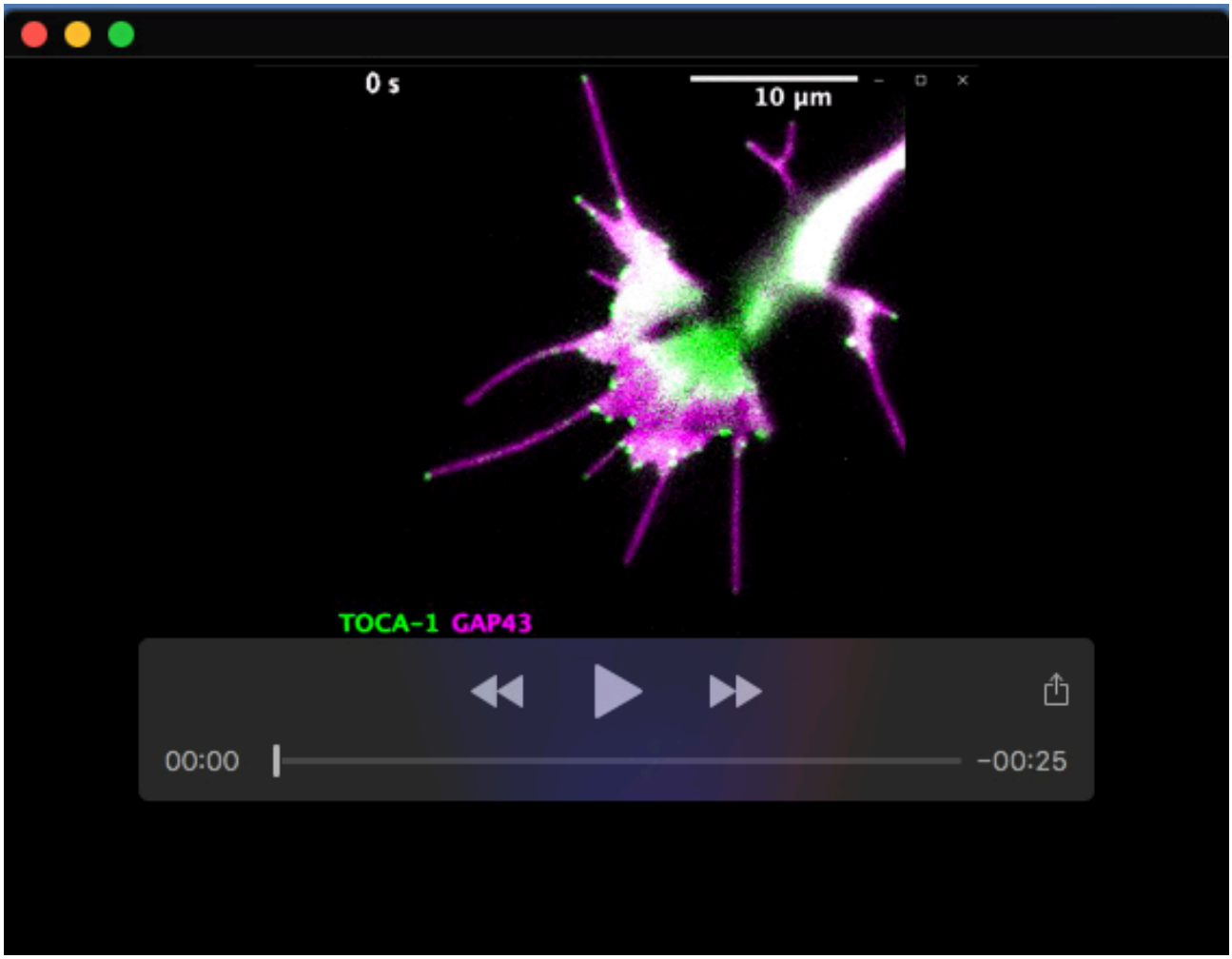

Movie 1. RGC growth cone expressing mNG-TOCA-1 and GAP43-RFP, showing TOCA-1 recruitment to filopodia, lamellipodia and inwardly-moving puncta. 4 minute video acquired at 2 s per frame, replayed at 20 frames per second.

Journal of Cell Science • Supplementary information

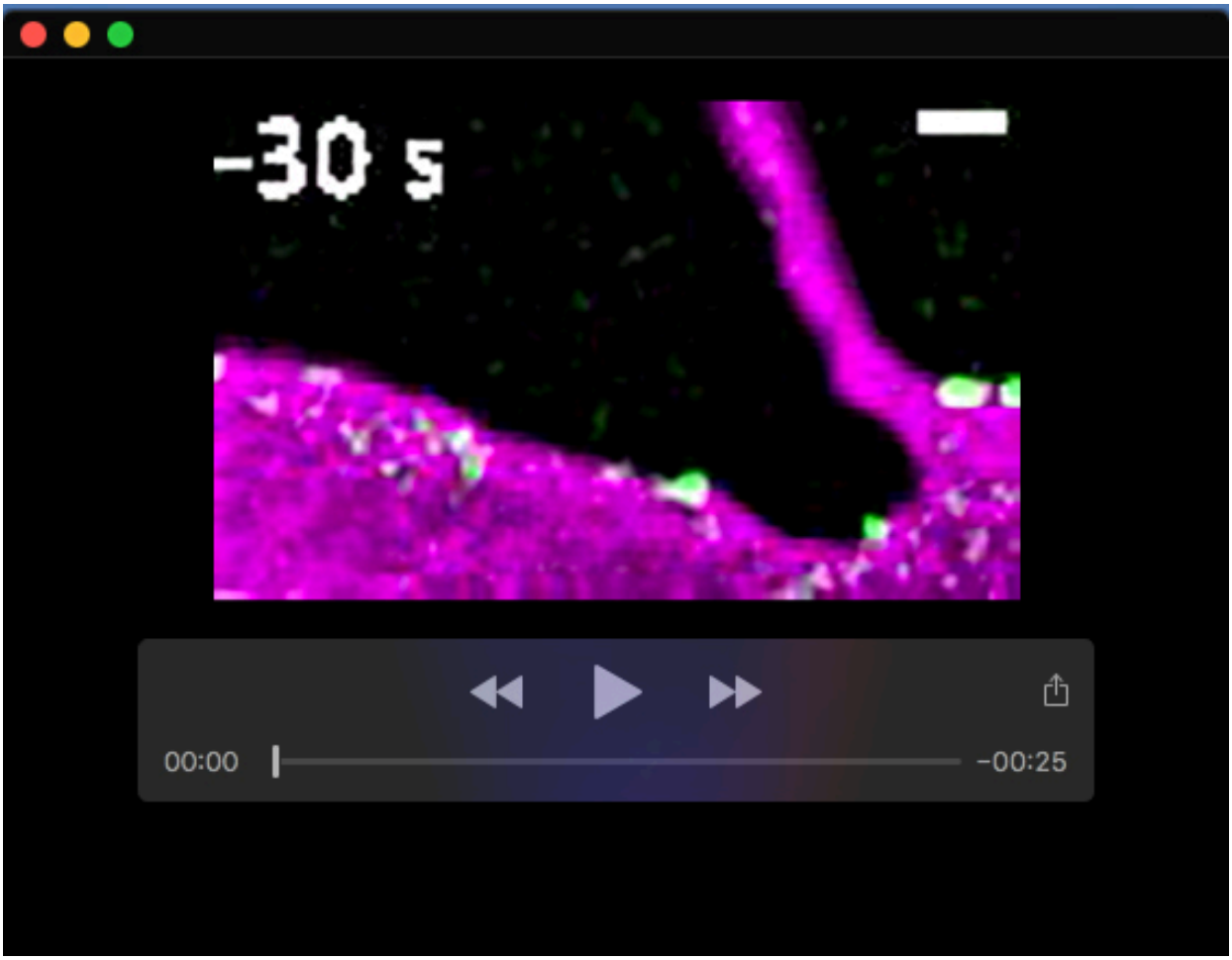

Movie 2. RGC growth cone expressing mNG-TOCA-1 (green) and GAP43-RFP (magenta), showing detail of filopodium formation, with two puncta of mNG-TOCA-1 moving laterally on the plasma membrane and coalescing before initiation. Image de-noised with nd-safir. Time relative to filopodium formation, scale bar 1 µm. 1 minute video acquired at 2 s per frame, replayed at 4 frames per second.

Journal of Cell Science • Supplementary information

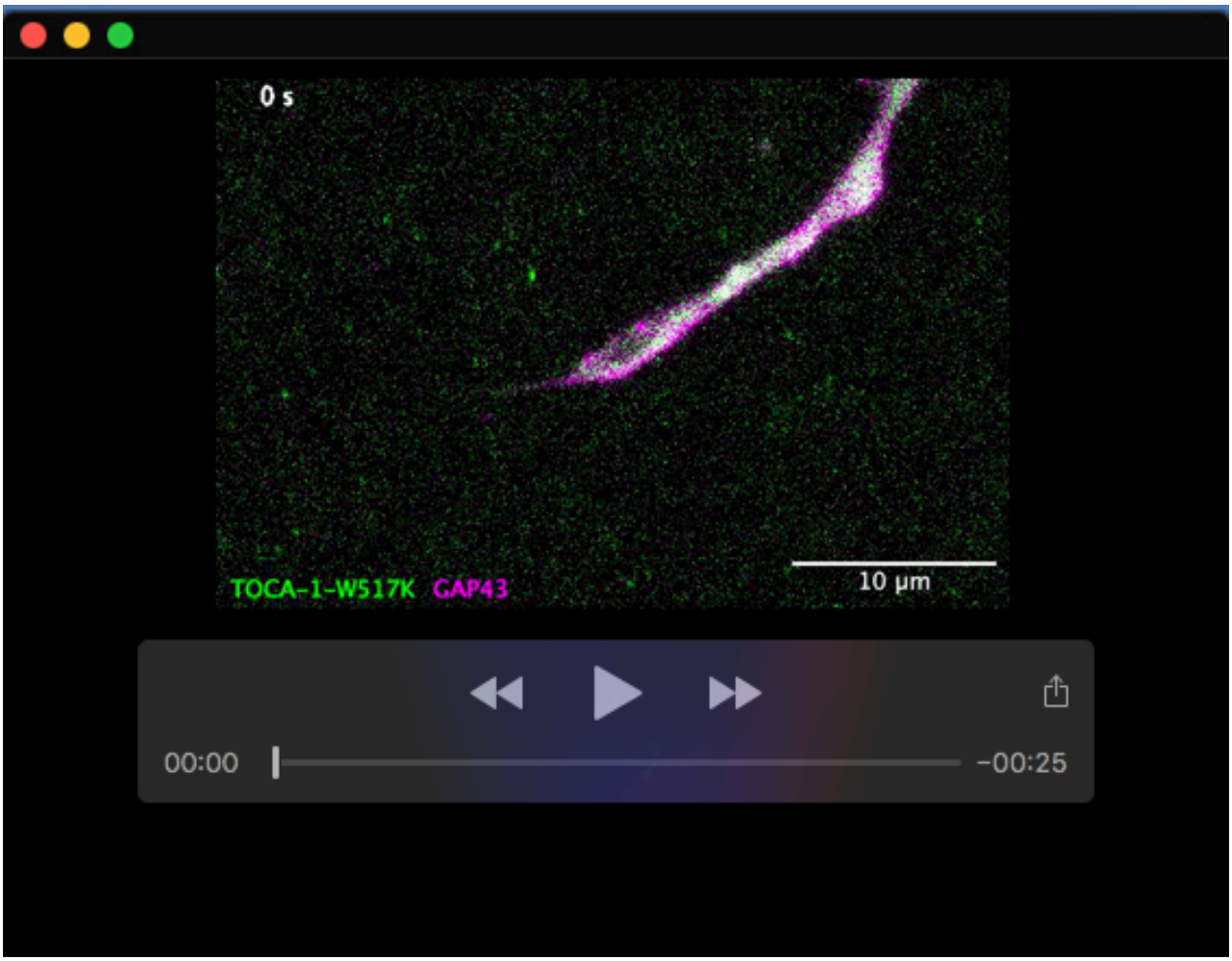

Movie 3. RGC growth cone expressing mNG-TOCA-1-W517K and GAP43-RFP, showing more diffuse TOCA-1 puncta with reduced enrichment of TOCA-1 to filopodia. 3 minute video acquired at 1.5 s per frame, replayed at 20 frames per second.

Journal of Cell Science • Supplementary information

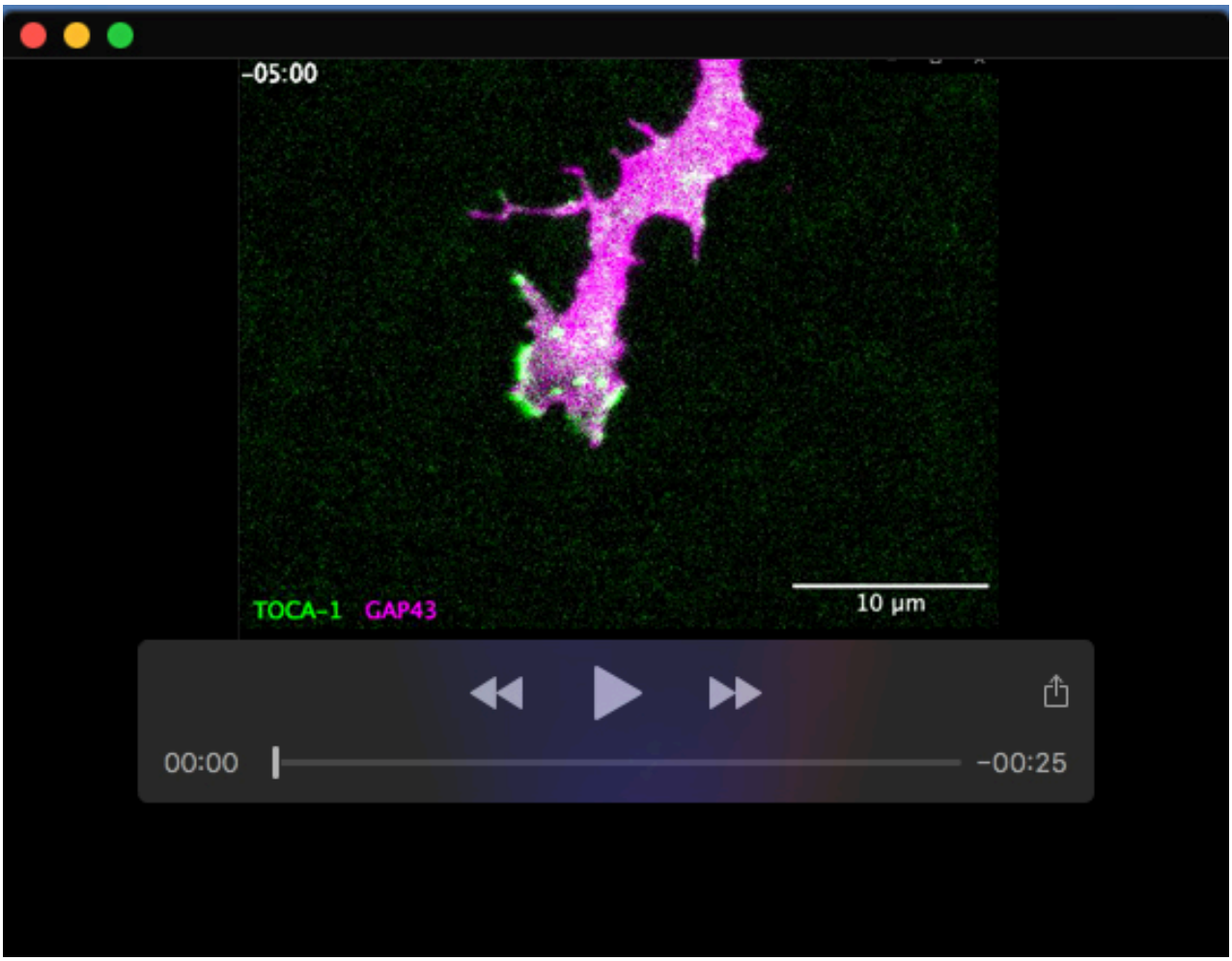

Movie 4. RGC growth cone expressing mNG-TOCA-1 and GAP43-RFP after treatment with 3.16 µM CASIN at t = 0, showing cessation of filopodia and lamellipodia activity by 10 minutes post-treatment, and coincident loss of TOCA-1 fluorescence. 25 minute video acquired at 7.5 s per frame, replayed at 20 frames per second, time shown in mm:ss.

Journal of Cell Science • Supplementary information

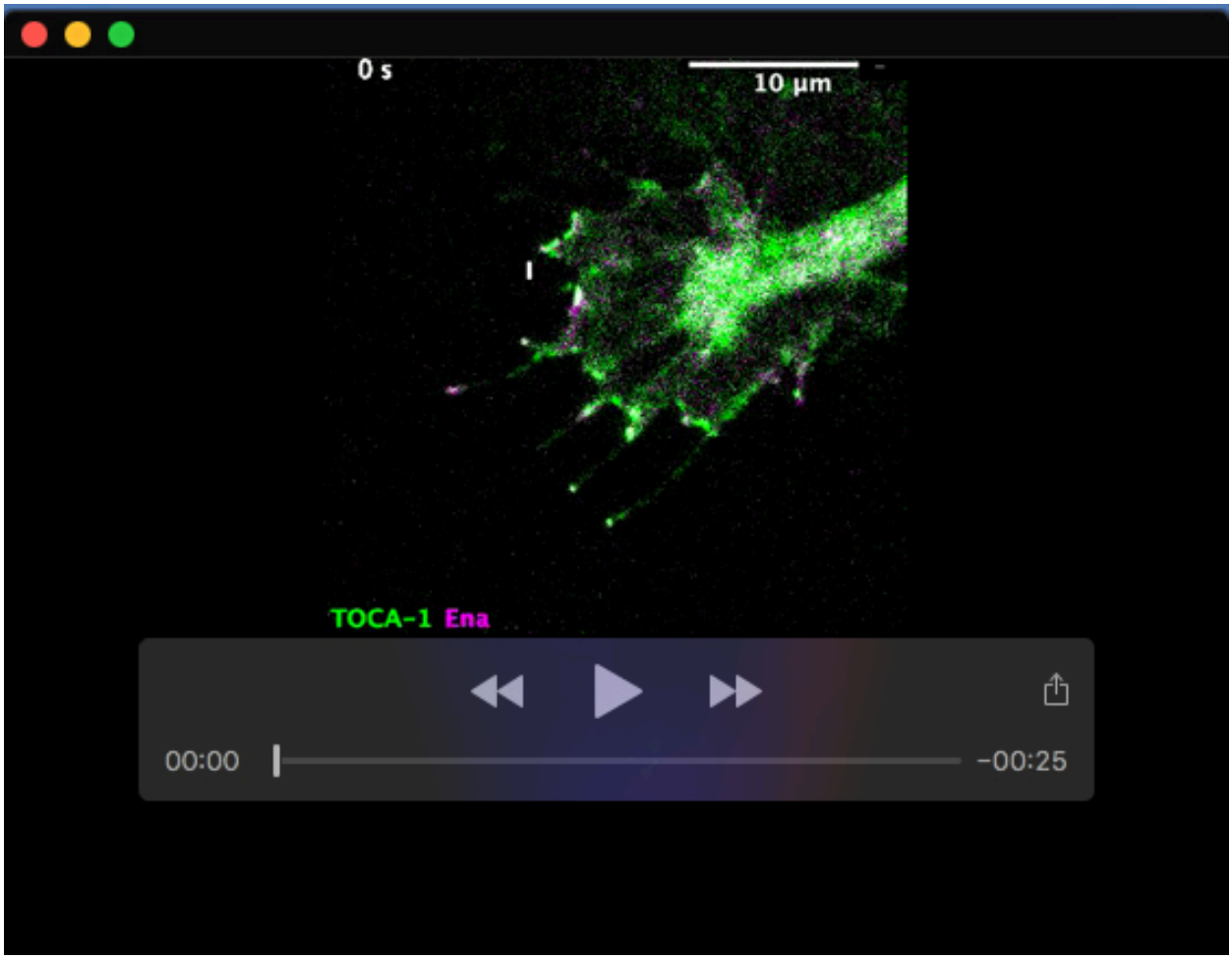

Movie 5. RGC growth cone filopodium expressing mNG-TOCA-1 and mScarlet-Ena, showing that the two proteins coincide during filopodial protrusion events (I = initiation, M = re-extension after merging, L = re-extension after lamellipodium catching up with filopodium). 3 minute video acquired at 1.5 s per frame, replayed at 10 frames per second.

Journal of Cell Science • Supplementary information